Quantum Review Letters 2 (2026) 143–160

Contents lists available at ScienceDirect

Quantum Review Letters

journal homepage: www.elsevier.com/locate/qrl

Review

Quantum effects in natural photosynthesis: From molecular architecture to design principles for artificial light-energy conversion

Kai-Ya Zhang [a], Rui Li [a], Yi Li [a], Ming-Zi Jin [a], Rong-Hang Chen [b,*], Qing Ai [a,*]

[a] School of Physics and Astronomy, Beijing Normal University, and Key Laboratory of Multiscale Spin Physics (Beijing Normal University), Ministry of Education, Beijing, 100875, China

[b] Beijing Computational Science Research Center, Beijing, 100193, China

ARTICLE INFO

Keywords:
Photosynthesis
Energy transfer
Structural features
Quantum coherence
Vibronic coherence
Artificial photosynthetic system

ABSTRACT

Photosynthesis is a central biochemical process, which converts solar energy into chemical energy and supports life on Earth. This review elucidates the relationship among structural features, quantum mechanisms and energy transfer efficiency in both oxygenic and anoxygenic phototrophs. We examine how different geometric configurations of light-harvesting complexes optimize energy transfer efficiency through electronic coupling and vibronic coherence. The review highlights the principles, energy gradient and clustered arrangement, that govern these effects and discusses common computational methods for evaluating energy transfer efficiency in photosynthetic systems. Drawing inspiration from the geometric architectures of natural photosystems, we discuss how these principles may guide the design of artificial photosynthetic systems, focusing on the strategic tuning of structural parameters to enhance quantum-mediated energy transfer. This theoretical framework emphasizes the importance of chromophore arrangement, electronic coupling, and environmental interactions in improving energy capture and conversion efficiency. Finally, we consider future directions, stressing the need for a clearer understanding of how these structural features can be translated into synthetic systems. Future research should help narrow the gap between natural and artificial photosynthetic systems, and support the development of sustainable energy technologies.

1. Introduction

Photosynthesis is one of the most important biochemical processes on Earth, converting solar energy into chemical energy and providing the foundation for almost all life forms. Oxygenic phototrophs, including plants, algae, and cyanobacteria, employ specialized photosynthetic architectures for harvesting solar energy. In contrast, anoxygenic phototrophic bacteria employ different photosynthetic architectures as reflected in their distinct reaction centers and antenna systems. Mirkovic and Scholes [1] provided schematic diagrams of light-harvesting structures across different organisms. Whether in simple bacteria and algae or in complex higher plants, many photosynthetic complexes exhibit a common three-part structural model consisting of an antenna, transfer network, and reaction center [2]. In most well-characterized photosynthetic systems, light energy is captured by the antenna, transferred to the reaction center via an exciton mechanism, and converted into chemical energy through photochemical reactions [3–5]. Quantum effects in light harvesting were comprehensively reviewed by Engel et al. [6], and the quantum characteristics of these processes were further elaborated by Panitchayangkoon et al. [7],Collini et al. [8], Fassioli et al. [9]. The initial light-harvesting and excitation-energy-transfer processes of photosynthesis can achieve near-unity quantum efficiencies, a remarkable feature that has attracted extensive research interest [10]. Significant progress has been made in elucidating the fine structure of photosynthetic complexes, the EET processes within these complexes, and the role of quantum effects in photosynthesis [6,8,11–14]. Numerous studies have revealed that photosynthetic structures either exploit quantum effects or use structural organization to influence energy transfer efficiency [15–21]. This raises the question of how the spatial and energetic structure of photosynthetic complexes contributes to EET, trapping, and the high quantum yields observed in natural light-harvesting systems.

In natural photosynthetic antennae, an important structural feature is the energy gradient, or the energy funnel, which refers to the arrangement of pigments in a manner that creates a gradient of excitation

* Corresponding authors.
E-mail addresses: chenronghang@csrc.ac.cn (R.-H. Chen), aiqing@bnu.edu.cn (Q. Ai).
URL: https://quanphys.bnu.edu.cn/ (Q. Ai).
Peer review under the responsibility of Editorial Board of Quantum Review Letters.

https://doi.org/10.1016/j.qrl.2026.07.003
Received 30 April 2026; Received in revised form 30 June 2026; Accepted 23 July 2026

Abbreviations

2DES	Two-dimensional electronic spectroscopy
A	acceptor
ATP	adenosine Triphosphate
ACPII	Alloxanthin–chlorophyll *a*/*c*-binding protein II
B	bridge
B800	B800 bacteriochlorophyll ring
B850	B850 bacteriochlorophyll ring
BChl(s)	Bacteriochlorophyll(s)
CDC	Charge density coupling
Chl(s)	chlorophyll(s)
CMRT	Coherent modified Redfield theory
CP	Chlorophyll protein
D	donor
D1/D2	D1/D2 reaction-center proteins of photosystem II
DNA	deoxyribonucleic acid
E. coli	Escherichia coli
EET	Excitation energy transfer
ETC	Electron transfer chain
FCP	fucoxanthin–chlorophyll a/c-binding protein
FMO	Fenna–Matthews–Olson
FRET	Förster resonance energy transfer
GSB	Green sulfur bacteria
H.c.	Hermitian conjugate
HEOM	Hierarchical equations of motion
LH1	light-harvesting complex 1
LH2	light-harvesting complex 2
LHC	Light-harvesting complex
Lhca	Light-harvesting chlorophyll a/b-binding protein
LHCI	Light-harvesting complex of photosystem I
LHCII	Light-harvesting complex of photosystem II
MOF	metal–organic framework
NADPH	reduced nicotinamide adenine dinucleotide phosphate
NMQT	non-Markovian quantum trajectory
NPQ	Non-photochemical quenching
P680	primary donor chlorophyll pair of photosystem II
P700	primary donor chlorophyll pair of photosystem I
PSI	Photosystem I
PSII	Photosystem II
PSII-SC	photosystem II supercomplex
RC	Reaction center
TDC	Transition density cube
TDDFT	Time-dependent density functional theory
TrEsp	Transition charge from electrostatic potential

energy levels, guiding the flow of excitation energy toward the reaction center. Another vital structural feature is the clustered arrangement of pigments. Generally, the mechanism of energy transfer in photosynthetic systems can be categorized into two types: incoherent hopping and coherent delocalization transfer [11,13,22], which are described by Förster resonance energy transfer (FRET) and Redfield theory, respectively (see Box 1 below). However, the actual energy transfer process in photosynthetic systems is more complex, and the two mechanisms often coexist [23,24]. The core parameters that determine the energy transfer mechanism are ratio of the electronic coupling strength against the energy gap between pigments [24]. Clustered pigment arrangements provide a useful structural basis for understanding this mixed coherent–incoherent transport picture. In the clusters, the pigments are closely spaced, leading to strong electronic coupling and the formation of delocalized excitonic states. While among the clusters, the pigments are distantly spaced, resulting in weaker coupling and a more localized excitation, which can be treated by the Förster theory. These two structural features can be found in various photosynthetic systems, such as the PSI and PSII supercomplexes in higher plants [25,26], the LH1 and LH2 complexes in purple bacteria [11,27], and the FMO complex in green sulfur bacteria [28,29]. Thus, it is reasonable to regard the two features as fundamental design principles in photosynthetic systems, both natural and artificial. To verify this hypothesis, we systematically review the relationship between these structural features and energy transfer efficiency across different photosynthetic systems, and also discuss the state-of-the-art and structure of artificial photosynthetic systems.

In this review, we first survey oxygenic and anoxygenic photosynthetic systems and summarize the geometric features of their light-harvesting complexes in Sections 2.1 and 2.2, with emphasis on energy gradients and pigment clustering. Then, we summarize the current understanding of the relationship between geometric structures and quantum effects in photosynthetic systems, with a particular focus on how these structural features influence energy transfer efficiency in Section 2.3. Next, we discuss how the design principles derived from natural photosynthetic systems can be applied to the development of artificial photosynthetic systems in Section 3. Finally, in Section 4, we discuss future research directions in this field, highlighting the need for a deeper understanding of how these structural features can be effectively translated into synthetic systems to bridge the gap between natural and artificial photosynthesis.

2. Revealing quantum efficiency in photosynthesis

Throughout this review, we distinguish among excitation-energy-transfer efficiency, trapping efficiency, photochemical quantum yield, and overall solar-to-chemical conversion efficiency. EET efficiency refers to the probability or fraction of an excitation reaching a specified acceptor or trap within a defined time window, whereas photochemical quantum yield denotes the fraction of absorbed excitations that produce successful charge separation under specified conditions [13,64–66]. These quantities are related but are not interchangeable, and none should be interpreted as the overall solar-to-chemical conversion efficiency of photosynthesis [66,67]. Table 1 provides a comparative roadmap of the major photosynthetic architectures, their dominant structural control parameters, and the evidence supporting proposed quantum–mechanical contributions.

2.1. Research on oxygenic photosynthetic organisms

Oxygenic photosynthesis converts carbon dioxide into carbohydrates and other cellular components, with water molecules providing electrons through oxidation reactions. The process can be primarily divided into three stages. In the first stage, solar light energy is captured. In the second stage, the captured energy is used to produce ATP and reducing equivalents. In the third stage, carbon dioxide is converted into carbohydrates and other cellular components [68]. The first and second stages primarily occur in PSI and PSII, respectively, and quantum effects have been observed in these processes. Oxygenic photosynthetic organisms include plants, algae, and cyanobacteria. In plants, PSI and PSII are organized into distinct supramolecular assemblies.

PSI-LHCI is among the most efficient known photosynthetic reaction-center systems, exhibiting a high internal photochemical yield under conditions in which excitation trapping and charge separation dominate over loss channels. This exceptional efficiency arises from the

Table 1
Comparison of different photosynthetic systems.[a].

Type of photosynthesis	Complex	Major EET pathway	Structural features	Quantum effects/efficiency mechanisms	Common research methods
Oxygenic	PSI-LHCI	LHCI/peripheral antennae → PSI core chlorophylls → RC (P700). red chlorophylls extend absorption into the low-energy region but can slow equilibration and excitation trapping.	In higher plants, four Lhca subunits form two heterodimers, Lhca1/4 and Lhca2/3, arranged as a crescent-shaped antenna belt around the PSI core. Pigment arrangement and orientation balance strong electronic coupling with avoidance of concentration quenching; red chlorophylls create low-energy states.	PSI exhibits a near-unity internal photochemical quantum yield, supported by rapid excitation transfer and charge separation. Protein-controlled pigment energies and couplings, together with excitonic delocalization, contribute to the energy-transfer landscape. Red chlorophylls introduce a trade-off between expanded spectral coverage and trapping kinetics.	2DES, structure-based Redfield–Förster modeling, combined structural and spectroscopic analysis/modeling, Modified Redfield, HEOM.
	PSII-SC	LHCII/minor antennae → CP43/CP47 core antennae → RC (D1/D2, P680). Excitation energy follows multiple, partially parallel routes rather than a simple energy-funneling pathway	The supercomplex comprises a dimeric PSII core with major LHCII and minor antenna complexes. CP43/CP47 serve as core antennae that mediate excitation delivery to the reaction center, sparse and spatially separated linker pigments limit electronic connectivity between peripheral antennae and the RC.	Coherent and incoherent contributions can coexist in descriptions of excitation-energy transfer. However, functional interpretations of long-lived electronic coherence in the intact PSII-SC should be made cautiously. Protein/environmental dynamics can regulate excitation migration and trapping and are incorporated in current models. However, the geometric structural determinants of PSII efficiency remain incompletely resolved.	Time-resolved fluorescence/absorption spectroscopy, structure-based quantum-dynamics modeling, and network analysis, kinetic Monte Carlo simulations, and Förster/Redfield/HEOM approaches.
Anoxygenic	FMO	Chlorosome → baseplate → FMO → RC;	FMO is a homotrimeric pigment–protein complex; depending on species and structure, each monomer binds seven or eight BChl *a* molecules. BChl 8 lies on the baseplate-facing input side, whereas BChls 1 and 6 are commonly treated as candidate input-side sites. BChl 3, together with nearby BChl 4, defines the RC-facing low-energy output region; BChl 3 is often treated as a principal terminal site. The protein-shaped site-energy landscape biases transfer toward the output region, while local pigment-pair geometry can tune electronic coupling.	Quantum coherence and environment-assisted transport have been extensively investigated in FMO. The protein scaffold tunes site energies and biases net transfer toward the RC-facing low-energy region. However, the functional role and the electronic versus vibronic origin of long-lived oscillatory signals remain debated.	2DES, HEOM, CMRT/Redfield theory, site-energy calculations, and open-quantum-system modeling.
	LH2 → LH1 → RC	LH2 (B800 → B850) → LH1 (B875/B880, species-dependent) → RC special pair.	In LH2, the B850 ring is strongly coupled, whereas the B800 ring is more weakly coupled. Ring symmetry, local dimerization, and pigment orientations shape electronic coupling and the excitonic-state structure, including access to dark states. LH1 contains multiple bacteriochlorophylls arranged around the RC in closed, elliptical, or partially open assemblies, depending on the species. LH1 geometry can influence intercomplex coupling.	Delocalized B850 excitons and dark-state protection can enhance transport in densely packed LH2 arrays, although their relevance in natural membranes remains unresolved. B800 coherence can affect B800 → B850 transfer robustness, and single-molecule experiments resolve room-temperature coherent pathways. Strong LH1 coupling supports exciton delocalization; idealized elliptical LH1–LH2 models can promote high-energy entangled states and heat-pump-like EET.	Structural spectroscopy, quantum master equations, Redfield/Förster/HEOM/modified Redfield approaches, mesoscopic diffusion and kinetic models, single-molecule ultrafast spectroscopy.

[a] The PSI-LHCI section refers to [25,30–36]; The PSII-SC section refers to [16,19,26,37–45]; The FMO section refers to [6,7,22,23,28,29,46–54]. The LH2-LH1-RC section refers to [11,12,27,52,53,55–63];

intricate pigment arrangement and energy transfer pathway organization. When the intermolecular distance between pigment molecules is sufficiently small, excitonic effects dominate, leading to delocalization of excited states across different pigment molecules. However, if the distance becomes too small, concentration quenching effects reduce quantum efficiency. Consequently, the pigments in PSI have evolved to achieve an optimal distance distribution within the permissible range [36,69]. This distribution is closely related to the protein structure, where proteins serve as scaffolds and regulate pigment energy, enabling the geometric configuration of pigments to reach an optimal state, thereby enhancing energy transfer rates while preventing excited-state quenching [70].

LHCI is composed of Lhca complexes that are arranged in a crescent shape surrounding the core structure of PSI. The Lhca complexes consist of chlorophyll *a*/*b*-binding proteins and exist as functional dimers of Lhca1/4 and Lhca2/3. The dimeric form of Lhca complexes exhibits greater stability, whereas the monomeric form leads to partial loss of pigments. Changes in conformation can influence photosynthetic efficiency by affecting pigment interactions and excitation energy transfer processes [33].

Particularly noteworthy is the presence of "red forms" of chlorophylls in PSI, which are found in virtually all PSI complexes [71]. Their excited-state energy in higher plants is lower than that of the reaction center [72]. Although these red forms reduce the rate of excitation energy transfer, they can broaden the absorption spectrum and protect the reaction center from photodamage [31]. Akhtar et al. [25] employed the combination of Redfield and Förster theory to compute the excitation dynamics of a structure-based model, and the resulting excitation energy transfer processes in PSI are illustrated in Fig. 1.

PSII in higher plants typically exists as a core dimer, which contains around 35 chlorophyll *a* molecules, and assembles with the major LHCII trimer and minor antenna proteins (CP24, CP26 and CP29) to form a PSII-SC. Excitations harvested by peripheral LHCII complexes are funneled toward the CP43/CP47 core antennas and the D1/D2 reaction-center region through several largely parallel transfer routes [37,73]. CP43 and CP47 cooperatively enhance both electronic energy transfer and charge separation, thereby improving the quantum efficiency of charge separation in the reaction center [42]. Compared with the near-unity quantum efficiency reported for PSI supercomplexes, excitation-energy delivery in higher-plant PSII-SC is markedly less efficient. A principal structural origin is the sparse and spatially separated set of "linker" pigments that couple the peripheral antenna to the PSII reaction center, which limits electronic connectivity between the antenna manifold and the primary donor. This architecture has been suggested to mitigate the risk of inadvertent oxidation of antenna chlorophylls by the unusually high oxidizing potential associated with the primary donor in PSII [38]. Furthermore, Shibata et al. [43] indicates that the simple funnel system fails to adequately explain the light-harvesting process in PSII. Although considerable progress has been made in excitation energy transfer network analysis based on PSII structures [26], definitive research findings regarding the geometric structural factors that influence photosynthetic efficiency remain scarce [74]. The schematic diagram of the EET in PSII is shown in Fig. 2. Zhang et al. [75],Wang et al. [76],Shen et al. [77] have investigated the EET processes in algae and cyanobacteria based on photosynthetic system structures. However, specific research on the relationship between geometric structures and quantum effects remains lacking.

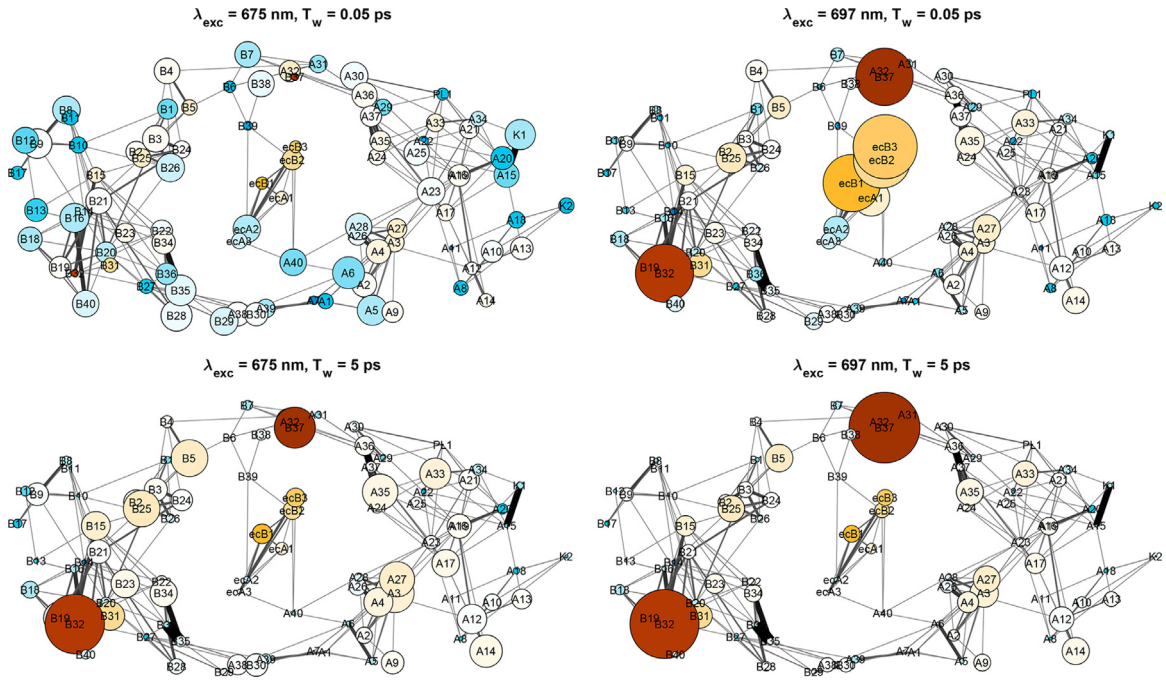

Fig. 1. Schematic of the structure-based Redfield–Förster model of EET in PSI. The size of the circles represents the population of individual Chls in the excited state, with the color of the circles indicating the chlorophyll energy levels. Blue circles correspond to higher-energy Chls, while red circles represent lower-energy red Chls. The lines represent EET between chlorophylls, with the line thickness indicating the energy transfer rate. Excitation sources at 675 nm and 697 nm were used, and the chlorophyll excited state populations were recorded at 50 fs and 5 ps after excitation with each light source.
Source: Figure adapted with permission of [25].

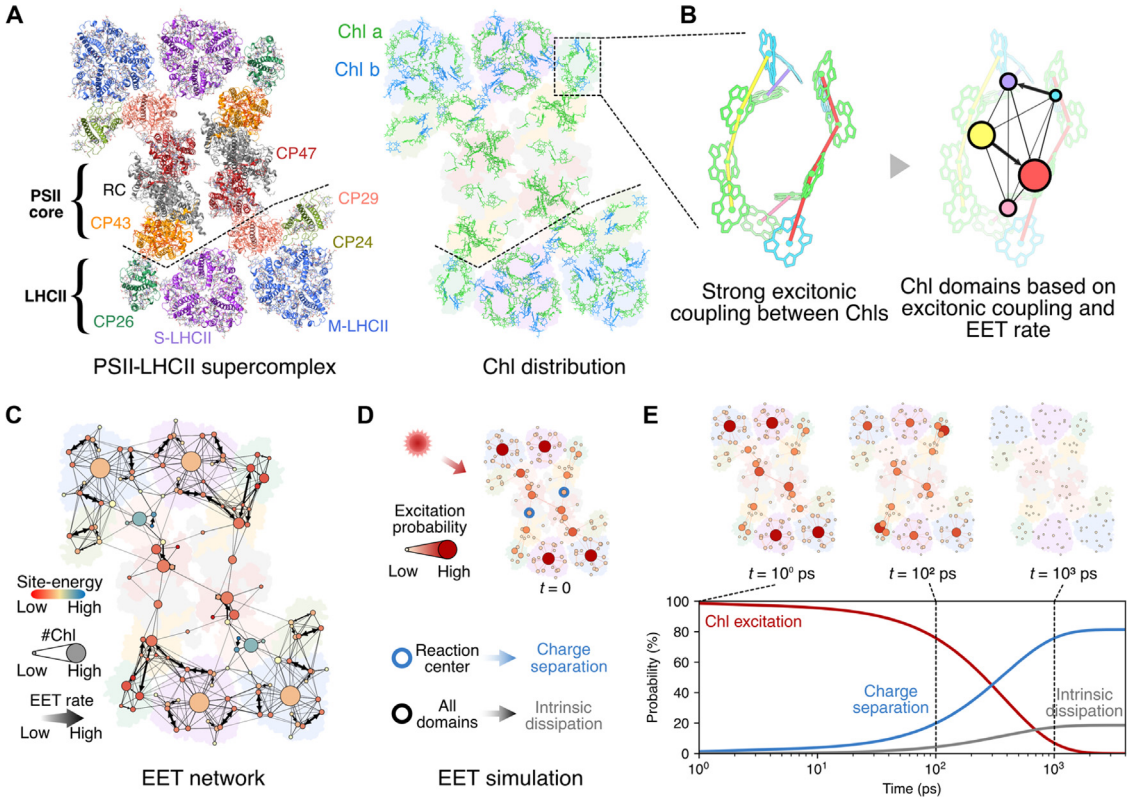

Fig. 2. EET analysis based on the PSII structure. A shows the protein composition and chlorophyll distribution of the PSII-SC. B illustrates the chlorophyll domain structure generated by exciton coupling. C depicts the EET process in PSII along with site energies, where the circle size represents the chlorophyll population, the circle color indicates the average site energy of the chlorophyll, and the arrow thickness represents the relative rate of EET. D illustrates the excitation probability of the structural domains due to random chlorophyll excitation caused by the special charge separation and intrinsic dissipation of chlorophyll at t = 0. E shows the probability distribution of chlorophyll excited states, charge separation, and intrinsic dissipation after initial excitation.
Source: Figure adapted with permission of [26].

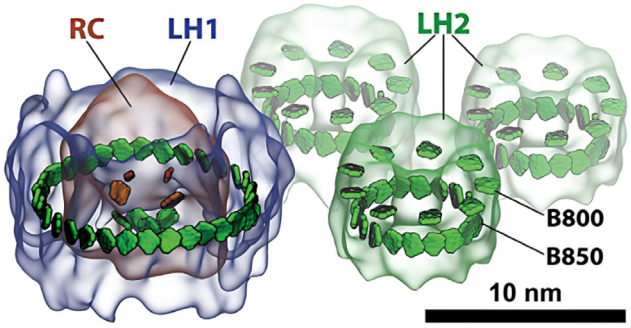

Fig. 3. Schematic diagram of the LH1-RC complex and the surrounding LH2, along with their spatial distribution.
Source: Figure adapted with permission of [11].

These comparisons point to two different structural solutions to efficient light harvesting in PSI and PSII. In PSI, a densely connected chlorophyll network, together with a protein-tuned distribution of low-energy states, enables fast equilibration and efficient trapping in the reaction center. PSII is organized differently. Its antenna-to-core architecture is more heterogeneous and more tightly constrained by photoprotection. Excitations reach the reaction center through several partially parallel routes, while weak inter-complex connectivity and the competition between charge separation and dissipation shape the observed dynamics. The contrast between PSI and PSII is therefore best framed in terms of excitation migration, trapping kinetics, and photoprotective constraints, rather than as a simple ranking of overall quantum efficiency [13,19,20].

2.2. Research on anoxygenic photosynthetic organisms

Anoxygenic phototrophic bacteria, such as purple bacteria and green sulfur bacteria, employ photosynthetic architectures that are fundamentally distinct from those of oxygenic phototrophs. These organisms typically possess a single photosynthetic system, in contrast to oxygenic photosynthetic organisms, which harbor two distinct photosynthetic systems, PSI and PSII. Furthermore, anoxygenic phototrophic bacteria do not employ H_2O as an electron donor and consequently do not generate oxygen as a byproduct of photosynthesis [66].

The photosynthetic architectures of purple bacteria primarily consist of the peripheral LH2 antenna complex, the LH1-reaction center core complex, and the RC, as shown in Fig. 3.

The LH2 complex exhibits a ring-shaped architecture composed of nine pairs of $\alpha\beta$-apoproteins and contains two major pigment rings, namely the B800 ring and the B850 ring. Upon absorption by the B800 ring, light energy is subsequently transferred to the B850 ring and then relayed to LH1 [55]. In the B850 ring, 16–18 bacteriochlorophyll molecules are tightly packed with specific orientations, generating extremely strong intermolecular coupling effects. In contrast, the B800 ring contains 8–9 bacteriochlorophyll molecules arranged in a more loosely packed configuration, exhibiting weaker coupling interactions as shown in Fig. 4.

The absorption peak of the B800 ring remains consistent with that of isolated bacteriochlorophyll molecules, whereas the absorption peak of the B850 ring undergoes significant spectral shifts due to strong intermolecular coupling and interactions between the chromophores and the surrounding protein matrix [9]. The geometric configuration of B850 forms a system composed of approximately degenerate and strongly coupled sites, making it a focal point of research [78]. The B850 structure harnesses quantum effects to construct a highly efficient light-harvesting system, where the pigment molecules arranged in a ring configuration with large in-plane transition dipole moment components exhibit strong symmetry. This symmetry results in the transition

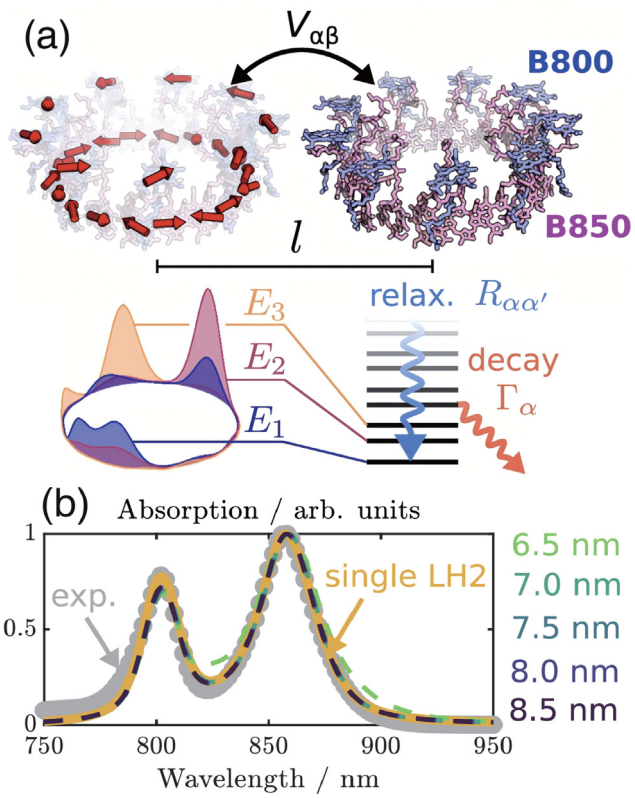

Fig. 4. Excitons in bacterial light-harvesting units. (a) Pigment arrangement in LH2, with the red arrows indicating the Q_y transition dipole moments, together with a schematic illustration of the partial delocalization and relaxation of electronic excitation. (b) Experimental absorption spectrum (gray dots) and the theoretical fit to the B800 and B850 bands in LH2.
Source: Figure adapted with permission of [27].

probability of the lowest degenerate state pair being N times stronger than that of all other excitonic states, where N represents the number of dimers in the ring. Upon excitation of one energy level, rapid relaxation occurs to the lowest excitonic state with minimal transition probability back to the ground state, thereby allowing the excitation energy to be confined for an extended duration [56,79–81]. This confinement reduces the generation of non-productive fluorescence and consequently enhances the energy transfer efficiency. Mattioni et al. [27] demonstrated that the local geometric organization within LH2 can modulate excitonic delocalization and the involvement of dark states, thereby enhancing long-range energy transport in densely packed LH2 arrays. However, whether this mechanism constitutes the primary origin of the improved energy-transfer efficiency observed in natural LH2 membranes remains inconclusive. Although electronic coupling in the B800 ring is relatively weak, Cheng and Silbey [58] showed that quantum coherence in this system is significant. This coherence can alter EET within LH2, and thereby can influence the uniformity and robustness of EET from B800 to B850 at room temperature.

LH1 is a bacteriochlorophyll-based core antenna associated with the reaction center; in different species, the spectral designation (e.g., B875 or B880) and assembly geometry of LH1 can vary, including closed, elliptical, and partially open arrangements [55,60]. In the purple non-sulfur bacterium, the LH1 complex utilizes 32 BChl molecules to form a ring-like structure (B875), where the tightly packed arrangement of BChl molecules gives rise to strong electronic interactions between nearest-neighbor molecules. Consequently, the excitation energy can be coherently delocalized across the BChl network, and this quantum coherence facilitates the accelerated transfer of energy from LH1 to the reaction center [11]. Oka [59] proposed an ideal model in which

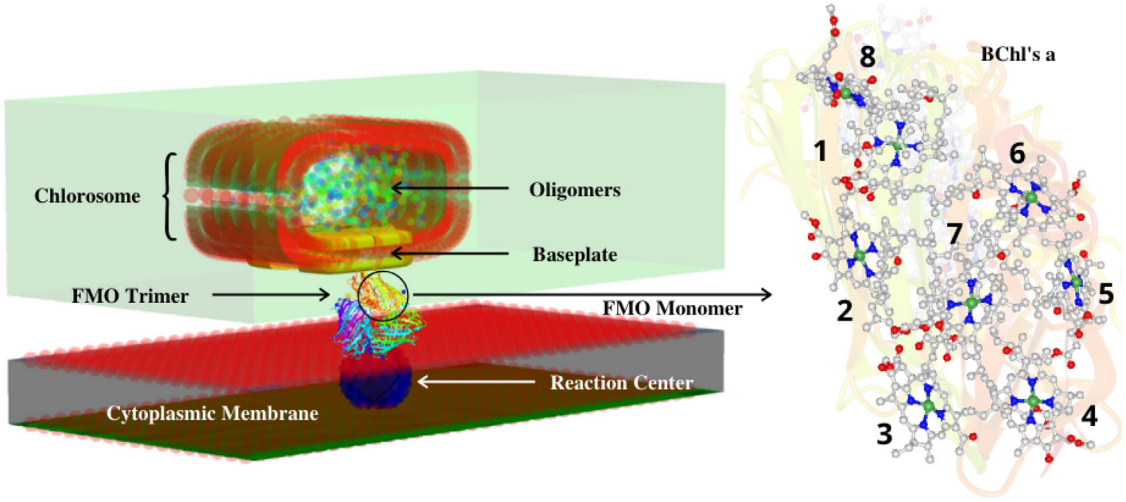

Fig. 5. Schematic diagram of the spatial arrangement of the chlorosome, the FMO protein, and the reaction center, along with the distribution of BChl in the FMO.
Source: Figure adapted with permission of [83].

the LH1 ring is not perfectly circular but adopts an elliptical geometry, and this structural deformation has important consequences for energy-transfer efficiency. The elliptical arrangement promotes the formation of quantum entanglement between LH1 and LH2 at higher excitation energies, enabling the utilization of thermal fluctuations to achieve a heat pump effect that facilitates highly efficient energy transfer from LH2 to LH1 via these high-energy quantum entangled states. The reaction center is positioned at the center of the LH1 ring structure. With the assistance of proteins, the reaction center preserves electronic coherence in photosynthetic complexes and facilitates the coherent spatial migration of excited states, which is crucial for maintaining the remarkable efficiency of photosynthetic energy conversion [15]. Policht et al. [82] identified the exciton and vibronic structures within the reaction center. Nevertheless, the mechanisms underlying their roles in energy transfer and charge separation still require further theoretical and experimental investigations. The photosynthetic architectures of green sulfur bacteria primarily consist of chlorosomes, the FMO protein, and the reaction center. The following schematic illustrates their structural configuration and spatial arrangement in Fig. 5.

Light is first absorbed by the pigments within the chlorosome, after which the resulting excitation energy is transferred to the baseplate and subsequently relayed from the baseplate to the FMO complex. The FMO protein complex is a key component of light-harvesting systems. It serves as a conduit for energy transfer between the chlorosomes and the RC, while chlorosomes act as light-harvesting antennae. The excitation energy transferred through the FMO complex is ultimately funneled to the RC, where the energy is used to drive photosynthetic processes [82].

The FMO complex is a water-soluble homotrimeric protein, with each monomer binding 7 or 8 bacteriochlorophyll *a* molecules. When the fine structure of the FMO complex was first studied, it was thought to contain only 7 BChls. Tronrud et al. [47] identified the presence of an eighth BChl within the FMO monomer. Subsequently, through computational analysis of the optical properties of the FMO protein, Schmidt am Busch et al. [48] demonstrated that this eighth BChl functions as a molecular bridge linking the FMO complex to the baseplate. BChls 1 and 6 have also commonly been treated as candidate input-side sites in exciton models of FMO, whereas BChl 3 and nearby BChl 4 are associated with the RC-facing output region [28,54]. Skochdopole and Mazziotti [84] proposed a quantum-redundancy picture for FMO, in which selected pigment subsystems can retain energy-transfer performance comparable to that of the full BChls. This quantum redundancy mechanism in nature can withstand the temporary or permanent loss of one or more chromophores. Subsequently, Moix et al. [49] found that the absence of the eighth BChl does not significantly alter the energy transfer efficiency. However, the optimal conditions for the bath parameters of the eight-BChl system are closer to experimental values compared to those of the seven-BChl system.

The FMO complex was among the earliest structurally characterized light-harvesting complexes [46]. Long-lived oscillatory signals have been observed in FMO spectroscopy, but their electronic versus vibronic origin and their functional relevance to energy-transfer efficiency remain debated [6,7,51,85,86]. The BChls within the FMO complex possess distinct site energies shown in Fig. 6, thereby establishing an energy gradient from higher- to lower-energy pigments, which directs excitation transfer from the baseplate-facing input side toward the reaction center-facing output region [54]. Adolphs and Renger [28] employed two independent methodologies to determine the site energies of the seven BChls within the FMO monomer and then calculated the spatial and temporal relaxation dynamics of excitons. Based on the computational results, it was concluded that the most significant factors influencing site energy variations are charged amino acids and ligands. Furthermore, the orientation of the FMO trimer relative to the RC positions BChl 3 and BChl 4 at the interface between the two complexes, thereby enhancing the efficiency of energy transfer. Ishizaki and Fleming [29] proposed that the FMO complex utilizes quantum coherence in conjunction with the protein scaffold-modulated site-energy landscape to guide the unidirectional energy flow from the chlorosome antenna to the RC. Thus, it can be speculated that quantum coherence enables the system to overcome local energetic traps, consequently improving the efficiency of energy transfer. Through investigation of the geometric distribution of BChl positions within the FMO complex, Ai et al. [22] demonstrated that the site-energy landscape forms an energy funnel structure oriented toward the RC. Moreover, the energy gap resulting from the lower site energy of BChl 3 relative to other sites supports highly localized excitonic states, which can prevent energy backflow and thereby enhance the efficiency of energy transfer toward the RC. Additionally, the geometric dimerization of BChls within the FMO complex modulates the degree of electronic coupling, thereby tuning the energy matching of excitonic states and further improving energy transfer efficiency.

Several structural themes run through anoxygenic light-harvesting systems. Pigment geometry sets the electronic couplings, site energies bias the direction of excitation flow, the protein environment modulates disorder and dissipation, and trapping at the reaction center turns migration into photochemical output. In purple bacteria, the LH2-LH1 architecture is shaped by ring-like pigment arrays, collective excitonic

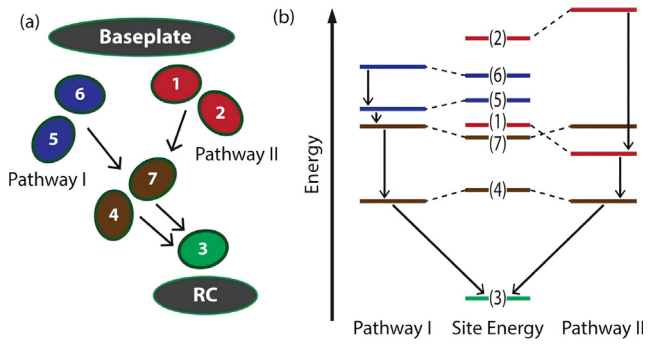

Fig. 6. (a) Dimeric arrangement of chlorophylls in the FMO monomer and the EET pathways. (b) Excitation energies of chlorophylls in the FMO and the energy transitions of the two EET pathways.
Source: Figure adapted with permission of [22].

states, and coupling between adjacent antenna complexes. FMO, by contrast, relies more on a protein-tuned energy landscape with defined input and output regions. From this perspective, quantum coherence is best regarded as a system-dependent dynamical feature. It is neither a stand-alone explanation for high efficiency nor a negligible by-product. Its contribution depends on the geometry, energy landscape, bath fluctuations, and trapping kinetics of the specific complex.

2.3. Structure-based quantum coherence: The origin of the near-unity efficiency

It is no doubt that the specific spatial arrangement of chromophores in light-harvesting antennae has a decisive impact on the efficiency of energy transfer [87,88]. However, it is still unclear how near-unity efficiency is determined by the spatial arrangement of chromophores and the quantum mechanism behind it. Quantum coherence, which is also called electronic coherence or electron exciton coherence, originates from the delocalization of the exciton eigen state of electron degree of freedom. For the restricted definition of quantum coherence, see Ref. [19]. The existence of quantum coherence in biological photosynthetic systems, specifically in the FMO complex found in green sulfur bacteria, was first reported in [6] with two-dimensional electronic spectroscopy, and soon verified by [7,50], theoretically and experimentally. Furthermore, Collini et al. [8] and Romero et al. [16] elucidated the existence and function of quantum coherence in cryptophyte marine algae and PSII RC, which further emphasized the importance of coherence in enhancing the quantum efficiency of the EET process. Nevertheless, an entirely distinct viewpoint of the long-lived coherence reported by [6] have been raised as early as 2012 [51], and have been summarized by [19,89]. This view argues that the observed long-lived coherence is not of electronic origin but rather arises from vibrational modes that are resonant with excitonic energy gaps [19,51,85,86,89]. In this subsection, we review the major works on this issue and discuss the controversies they have generated.

Several theoretical approaches are available for calculating the energy transfer efficiency of photosynthetic systems as open quantum systems with system–bath interactions as the origin of dissipation, including FRET, CMRT, and the numerically exact HEOM. In the box below, we provide a brief introduction to these methods, highlighting their respective domains of application and key advantages [90,91].

The structure-based quantum mechanism was first elucidated in LH1 and LH2 with a single or double ring structure. Yang et al. [57] investigated the influence of spatial factors on the quantum transfer efficiency and average transfer time. As introduced in Section 2.2, LH2 consists of two pigment rings, named B800 and B850, respectively. Note that no RC exists in LH2 and it serves as an energy transfer pathway to the RC in another complex, LH1. In this study, a double-ring XY-model was presented to simulate the LH2, and the results indicated that a specific dimerization of the B850 ring can promote the transfer efficiency and shorten the transfer time at the same time.

The model in [57] treated all BChls as two-level systems with excited states $|e_j^{[c]}\rangle$ and ground states $|g_j^{[c]}\rangle$ and excitation energy Ω_c, which is suitable only for the zero- and one-exciton subspaces. Thus, the raising and lowering operators of the jth BChl on the $[c]$ ring are

$$\sigma_j^{+[c]} = |e_j^{[c]}\rangle\langle g_j^{[c]}|, \quad \sigma_j^{-[c]} = |g_j^{[c]}\rangle\langle e_j^{[c]}|, \tag{11}$$

with $c = a(b)$ denoting the B800 (B850) ring. The Hamiltonian of B800 and B850 under the XY model reads

$$H_a = \frac{\Omega_a}{2}\sum_{j=1}^{N}\sigma_j^{z[a]} + J_1\sum_{j=1}^{N}(\sigma_j^{+[a]}\sigma_{j+1}^{-[a]} + \text{H.c.}) \tag{12}$$

and

$$\begin{aligned} H_b =& \frac{\Omega_b}{2}\sum_{j=1}^{2N}\sigma_j^{z[b]} + J_2\sum_{j=1}^{N}[(1+\delta)\sigma_{2j-1}^{+[b]}\sigma_{2j}^{-[b]} \\ &+ (1-\delta)\sigma_{2j}^{+[b]}\sigma_{2j+1}^{-[b]} + \text{H.c.}], \end{aligned} \tag{13}$$

with $N = 8$. In Eq. (13), the parameter $\delta \neq 0$ describes the dimerization of BChls in B850 rings. The interaction Hamiltonian between B800 and B850 could be written as

$$\begin{aligned} H_{ab} =& g_1\sum_{j=1}^{N}[\sigma_j^{+[a]}(\sigma_{2j-1}^{-[b]} + \sigma_{2j}^{-[b]}) + \text{H.c.}] + g_2\sum_{j=1}^{N}[\sigma_j^{+[a]} \\ &\times (\sigma_{2j-3}^{-[b]} + \sigma_{2j-2}^{-[b]} + \sigma_{2j+1}^{-[b]} + \sigma_{2j+2}^{-[b]}) + \text{H.c.}]. \end{aligned} \tag{14}$$

For the function of LH2, the final state of energy transfer in LH2 should be the ground state

$$|0\rangle \equiv \prod_{j=1}^{N}|g_j^{[a]}\rangle \otimes \prod_{j=1}^{2N}|g_j^{[b]}\rangle, \tag{15}$$

and the population on the ground state provides the energy transfer efficiency η. The other LH2 and LH1 complexes are regarded as the environment, and the physical picture here turns into energy leakage from LH2 to the environment.

In the following steps, a Markovian quantum master equation is used to obtain the numerical solution of η , as described in Box 1. While solving the master equation, they transformed the equation to the k-space and proved that the efficiency $\eta(t)$ of a mixed initial state $\rho(0) = \sum_{k_1,k_2}\rho_{Ak_1,Ak_2}(0)|A,k_1\rangle\langle A,k_2|$ is the weighted average of $\eta^{[A,k]}(t)$ whose initial states are $\rho^{[A,k]}(0) = |A,k\rangle\langle A,k|$ as

$$\eta(t) = \sum_k \rho_{Ak,Ak}(0)\eta^{[A,k]}(t). \tag{16}$$

The details of the derivation are demonstrated in Sec. III ∼ VI in [57]. Finally, the numerical result of η as function of time t and dimerization parameter δ is plotted as a contour map (see Fig. 5 of [57]), which indicates that in the short t regime of a practical energy transfer process, $\delta \neq 0$ can enhance the transfer efficiency due to the quantum coherence from dimerization of the B850 ring. The effect of dimerization as a result of a specific structure on transfer efficiency has also been investigated in other studies [22,60].

Furthermore, the energy transfer in LH1 has also been studied in Ref. [93], where a dark-state effect was identified to suppress the population on less important BChls to improve the energy transfer efficiency. They concentrated on a ring-shaped model consisting of a single acceptor at the center and several donors uniformly distributed on the circumference, which is similar to LH1. Following the convention, the donors are modeled as two-level systems, i.e., $|e\rangle$ and $|g\rangle$, with energy gap $\varepsilon_i (i = 1, \ldots, N)$. On the ring, only adjacent hopping of excitations is considered with coupling strength g. To simulate the absorption of sunlight, each BChl is supposed to be coupled to light of frequency ω, which is described by the creation (annihilation) operator $b^\dagger$ (b).

Box 1. Theoretical methods for EET in photosynthetic systems

Förster theory. Förster theory, proposed by Theodor Förster in 1948, describes a nearly-classical picture of resonance energy transfer, in which the energy transfer process is modeled as a random walk in a network of chromophore sites [13,92]. Energy transfer from the donor to the acceptor occurs via several hopping steps, each of which is induced by dipole–dipole interactions between the two chromophores under the weak coupling assumption. Given the nature of dipole–dipole coupling, the transfer rate k_{AB} between two specific sites A and B, which is the focus of our analysis, is reasonably proportional to $1/R^6$, where R denotes the inter-chromophore distance. The complete form of k_{AB} reads

$$k_{AB} = k_A \left(\frac{R_0}{R}\right)^6, \tag{1}$$

where k_A is the dissipation rate without B, and R_0 is the distance at which $k_{AB} = k_A$, known as the critical quenching radius or Förster radius. Förster obtained the expression of R_0 with the spectral overlap integral J, the quantum yield of the donor Φ_A, and the orientation factor κ as

$$R_0^6 = \frac{9(\ln 10)}{128\pi^5 N_A}\frac{\kappa^2 \Phi_A}{n^4} J, \tag{2}$$

where n is the medium index of refraction and N_A is the Avogadro constant. The spectral overlap integral J reflects the degree of overlap between the donor emission spectrum and the acceptor absorption spectrum, thereby guaranteeing energy conservation.
Förster theory, compared with the other two theories discussed here, has the advantages of simplicity and relatively accurate prediction in the incoherent regime. However, Förster theory, which is founded on the dipole-dipole interaction, becomes invalid when the inter-chromophore distance is on the same order as the chromophore size, i.e., when the coherence between chromophores is sufficiently strong. Under that condition, the transfer rate is strongly dependent on the spatial geometry of chromophores, thereby limiting the concise form of Förster theory.

Coherent modified redfield theory. Instead of the semiclassical form of Förster theory, CMRT is based on the equation that governs the total density matrix $\rho_{\rm tot}$ of the system and environment ($\hbar = 1$).

$$\dot{\rho}_{\rm tot} = -i[H, \rho_{\rm tot}]. \tag{3}$$

The total Hamiltonian is $H = H_S + H_B + H_{SB}$, with $H_S = \sum_{k,l} E_k|k\rangle\langle k| + J_{kl}|k\rangle\langle l|$ and H_B being a collection of harmonic oscillators, where E_k and J_{kl} are respectively the site energy and electronic coupling in the site basis $|k\rangle$. Here, $|k\rangle$ represents the state in which only the kth site is in its excited state and the other sites are in the ground states. The exciton states $|e_n\rangle$ satisfying $H_S|e_n\rangle = e_n|e_n\rangle$ can be expressed in the site basis $\{|k\rangle\}$ as $|e_n\rangle = \sum_k C_{nk}|k\rangle$. Since we are only interested in the population of the system, we can extract the reduced density matrix of the system ρ_S from ρ_{tot} by taking a partial trace over the bath degrees of freedom as

$$\rho_S = {\rm tr}_B(\rho_{\rm tot}). \tag{4}$$

The evolution of ρ_S is governed by the quantum master equation, which is written in the exciton basis $\{|e_n\rangle\}$. Using perturbation theory and the secular approximation, the form of the master equation is obtained as

$$\partial_t \rho_S = -i[H_S(t), \rho_S] - \sum_{n\neq n'} R^{\rm dis}_{nn'}(t)\left[\left\{\mathcal{A}^\dagger_{nn'}\mathcal{A}_{nn'}, \rho\right\} - 2\mathcal{A}_{nn'}\rho\mathcal{A}^\dagger_{nn'}\right] - \sum_{n\neq n'} R^{\rm pd}_{nn'}(t)\rho_{nn'}\mathcal{A}_{nn'}. \tag{5}$$

where $\{A, B\} = AB + BA$ is the anti-commutator and $\mathcal{A}_{nn'} = |e_n\rangle\langle e_{n'}|$ is the jumping operator. Each term in Eq. (5) has a distinct physical interpretation. The first term is the evolution controlled by the electronic Hamiltonian. The second and the third terms represent dissipation of eigenstate $|e_n\rangle$ and pure dephasing between eigenstate and ground state, corresponding to the diagonal and off-diagonal terms in the original equation. The rate matrices $R^{\rm dis}_{nn'}(t)$ and $R^{\rm pd}_{nn'}(t)$ are determined by the line shape function $g(n)$, spectral density $J(\omega)$ and reorganization energy λ_n of the system. The detailed derivation of Eq. (5) and the specific form of $R^{\rm dis}_{nn'}(t)$ and $R^{\rm pd}_{nn'}(t)$ can be found in [53]. Note that the rate matrices for dissipation and pure dephasing are both time-dependent, originating from the time integral from 0 to t contained in the equation. When introducing the Markovian approximation into our theory, the upper limit of this integral is extended to infinity [91]. This extension implies that, for times t beyond the characteristic timescale of the system–bath interaction, the rate matrices converge to steady-state values. Consequently, the numerical simulation is simplified without sacrificing accuracy.
Compared to FRET, the master equation of CMRT takes into account the effects of spontaneous emission and pure dephasing on the dynamics, thus providing higher numerical accuracy when treating the systems with strong coherence.

Without loss of generality, the site energies of donors are assumed to be identical, i.e., $\varepsilon_i = \varepsilon$. The Hamiltonian of this ring model reads

$$H = H_D + \varepsilon_A A^\dagger A + H_{DA} + \omega b^\dagger b + J\sum_{i=1}^{N}(e_i^\dagger b + {\rm H.c.}), \tag{17}$$

where $H_D = \sum_{i=1}^N [\varepsilon e_i^\dagger e_i + g(e_i^\dagger e_{i+1} + {\rm H.c.})]$ and $H_{DA} = \sum_{i=1}^N \xi(e_i A^\dagger + {\rm H.c.})$ are the Hamiltonian of the donors and their interaction with the acceptor, respectively. The operators $e_i^\dagger = |e\rangle_i\langle g|$ and $A^\dagger = |e\rangle_A\langle g|$ represent the creation operators of the jth donor and the acceptor, respectively.

Next, we transform to the eigenstate representation of the donor Hamiltonian H_D. The creation and annihilation operators of the eigenstate, in other words, the collective excitation mode, can be written as a Fourier transformation

$$e_j^\dagger = \sum_k e^{-ikj}\tilde{e}_k^\dagger/\sqrt{N}, \tag{18}$$

$$e_j = \sum_k e^{ikj}\tilde{e}_k/\sqrt{N}, \tag{19}$$

where k is the momentum of the collective excitation, and the summation is over $k_n = 2\pi(n-1)/N$, with $n = 1, \ldots, N$. The donor Hamiltonian

Box 1 (continued). Theoretical methods for EET in photosynthetic systems

Hierarchical equations of motion. Hierarchical equations of motion [52,61,62] provide an exact approach compared to FRET and CMRT. Due to the second-order perturbation used in the derivation, the CMRT master equation cannot describe the multi-photon transition processes, which play a role in incoherent FRET dynamics, as noted in [52]. Thus, HEOM is developed to address the need for a rigorous framework that reduces to these two limiting cases, coherent CMRT and incoherent FRET, under different conditions.

For this purpose, a series of hierarchically coupled auxiliary density operators $\{\rho_n\}$ is introduced into the HEOM, which represents fluctuations of electronic energy and dissipation of reorganization energy [52]. The subscript $\mathbf{n}$ represents the set of indices $\mathbf{n} = \{\{n_{10}, n_{11}, \cdots\}, \cdots, \{n_{N0}, n_{N1}, \cdots\}\}$ that defines the hierarchy level. The index of $\mathbf{n}^{\pm}_{mk}$ differs from $\mathbf{n}$ only by changing the specified n_{mk} to $n_{mk}+1$. The ρ_0 with $\mathbf{0} = \{\{0,0,\cdots\},\cdots,\{0,0,\cdots\}\}$ is identical to the reduced density operator ρ_S defined before. The specific form of HEOM, as the coupled equations with ρ_S and $\{\rho_n\}$, depends on the correlation function $C(t)$ of the system [61], and is therefore related to the spectral density of system–bath interaction $J(\omega)$. Under the commonly employed Drude spectral density

$$J(\omega) = \frac{\eta\gamma\omega}{\omega^2+\gamma^2}, \tag{6}$$

with η as the coupling strength, the correlation function has the exponential series form as

$$C(t) = \sum_{k=0}^{N} c_k \mathrm{e}^{-\gamma_k t}, \tag{7}$$

where $\gamma_0 = \gamma$ is the Drude constant and $\gamma_{k\neq 0} = 2k\pi/\beta$ are Matsubara frequencies, with $\beta = 1/k_B T$ denoting the inverse temperature. The coefficients are determined by the fluctuation–dissipation theorem as [14]

$$c_0 = \frac{\eta\gamma}{2}[\cot(\beta\gamma/2) - i], \tag{8}$$

and

$$c_{k\neq 0} = \frac{4k\pi\eta\gamma}{(2k\pi)^2 - (\beta\gamma)^2}. \tag{9}$$

Assuming that the initial state is the direct product, i.e., $\rho_{\mathrm{tot}}(0) = \rho_S(0) \otimes \exp(-\beta H_{\mathrm{B}})/Z$ with Z as the partition function of the bath, the specific form of the HEOM can be written as

$$\dot{\rho}_n = -\left(i\mathcal{L} + \sum_{m=1}^{N}\sum_{k} n_{mk}\gamma_k\right)\rho_n - i\sum_{m=1}^{N}\left[|l\rangle\langle l|, \sum_k \rho_{n^+_{mk}}\right] - i\sum_{m=1}^{N}\sum_k n_{mk}(c_k|l\rangle\langle l|\rho_{n^-_{mk}} - c_k^*\rho_{n^-_{mk}}|l\rangle\langle l|). \tag{10}$$

where $|l\rangle$ is the vector in site basis, and the number of hierarchy levels N determines the accuracy in practical simulations.

H_D is diagonalized by $\tilde{e}_k^\dagger(\tilde{e}_k)$ as

$$H_D = \sum_k (\varepsilon + 2\ g\cos k)\tilde{e}_k^\dagger \tilde{e}_k, \tag{20}$$

and the interaction term becomes

$$\begin{aligned} H_{DA} &= \sum_j \xi\left(\sum_k e^{ikj}\tilde{e}_k A^\dagger/\sqrt{N} + \mathrm{H.c.}\right), \\ &= \sum_k \xi\left(\frac{1}{\sqrt{N}}\sum_j e^{ikj}\right)\tilde{e}_k A^\dagger + \mathrm{H.c.} \end{aligned} \tag{21}$$

Owing to the symmetric structure of the ring, the summations $\sum_j e^{ikj}$ with $k \neq 0$ vanish. Thus, only the $k = 0$ term is left and Eq. (21) is simplified as

$$H_{DA} = \sqrt{N}\xi(\tilde{e}_0 A^\dagger + \mathrm{H.c.}), \tag{22}$$

which indicates that only the zero-mode excitation is coupled to the acceptor. Thus, the total Hamiltonian can be separated into two decoupled parts: $H' = H_D - (\varepsilon + 2\ g)\tilde{e}_0^\dagger\tilde{e}_0$ and

$$\begin{aligned} H_{\mathrm{eff}} =& \omega_0\tilde{e}_0^\dagger\tilde{e}_0 + \omega b^\dagger b + \omega_A A^\dagger A \\ &+ \sqrt{N}[(\xi\tilde{e}_0^\dagger A + J\tilde{e}_0^\dagger b) + \mathrm{H.c.}], \end{aligned} \tag{23}$$

where $\omega_0 = \varepsilon + 2\ g - i\kappa$ and $\omega_A = \varepsilon_A - i\Gamma$. Here κ and Γ are phenomenologically introduced as the dissipation rate of donors and the chemical reaction rate of the acceptor.

In the effective Hamiltonian (23), there are three main types of excitation states under the single-excitation subspace, denoted as $|1_D\rangle$, $|1_b\rangle$, and $|1_A\rangle$, respectively. The energy structure of H_{eff} could be described as a three-level Λ type system (see Fig. 1 (b) of [93]). In this well-studied model, the presence of a dark state can dramatically enhance the energy transfer efficiency [94]. The so-called dark state effect is understood as the quantum interference phenomenon that renders the system transparent to certain decay channels. In the present case, the energy is from the solar photons, thus the initial state is $|1_b\rangle$, and the desired final state is $|1_A\rangle$. The dark state here is an eigenstate of H_{eff} that has only a small coefficient on the irrelevant state $|1_D\rangle$ to maximize the transfer efficiency. The theoretical condition for the existence of a dark state channel is that energy detuning $\Delta = \omega - \varepsilon_A = 0$. These properties all agree with the numerical result in [93]. Setting the parameters above as $\varepsilon_A/\xi = 12, g/\xi = 0.3, \kappa/\xi = 0.1, \Gamma/\xi = 0.3, \varepsilon/\xi = 11.4$ and $J/\xi = 0.1$, the eigenstates at resonance $\omega = \varepsilon_A$ are

$$\begin{aligned} |E_1\rangle &\approx -0.995|1_b\rangle + 0.01i|1_D\rangle + 0.01|1_A\rangle, \\ |E_2\rangle &\approx 0.07|1_b\rangle + (0.7 + 0.03i)|1_D\rangle + 0.7|1_A\rangle, \\ |E_3\rangle &\approx 0.07|1_b\rangle + (-0.7 + 0.03i)|1_D\rangle + 0.7|1_A\rangle, \end{aligned} \tag{24}$$

Here, $|E_1\rangle$ is the dark state and the initial state can be rewritten with the eigenstates above as $|1_b\rangle = 0.995|E_1\rangle + 0.07|E_2\rangle + 0.07|E_3\rangle$, indicating that the component of the dark state in the initial state is near-unity under the practical condition $J \ll \xi$. The numerical simulation result of energy transfer efficiency η as a function of detuning Δ and the ratio of dissipation rate to chemical reaction rate κ/Γ illustrated in Fig. 7(b) shows that there is a maximum efficiency at $\Delta = 0$ regardless of the value of κ/Γ. In summary, the ring-shape structures of LH1 and LH2 induce quantum mechanisms of dimerization and a dark state channel, leading to the near-unity energy transfer efficiency.

The ring-structured complex could also be stacked into several layers, constructing a rod-like overall complex. Kim and Cao [95] has proposed a "stacked-disk rod" model to simulate the experiments of

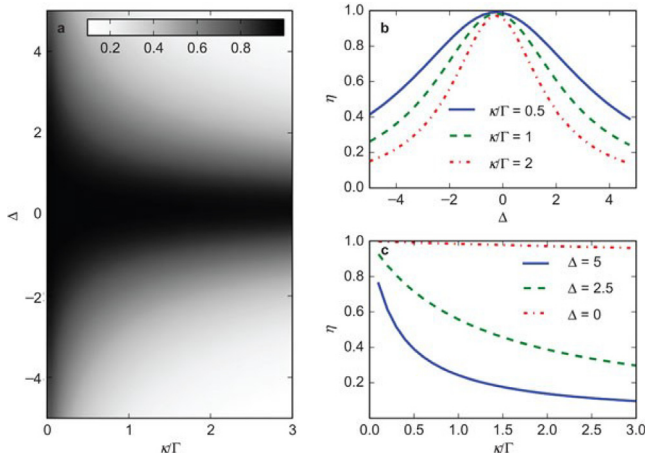

Fig. 7. (a) contour map of the transfer efficiency η depending on detuning Δ and the ratio κ/Γ. (b) and (c) are the section of (a) at different value.
Source: Figure adapted with permission of [93].

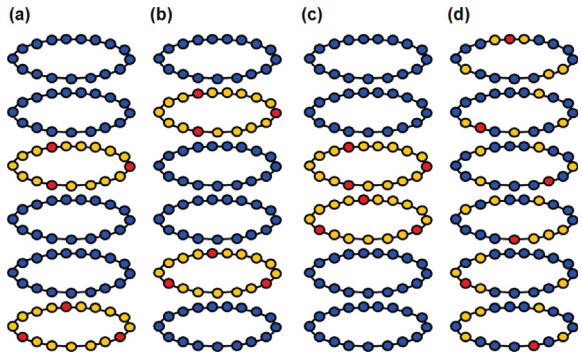

Fig. 8. Stacked-disk ABD rod system using in simulation of [95] with the ratio $N_d : N_B : N_A = 68 : 28 : 6$. The sites are arranged regularly in (a)~(c), and randomly in (d).
Source: Figure adapted with permission of [95].

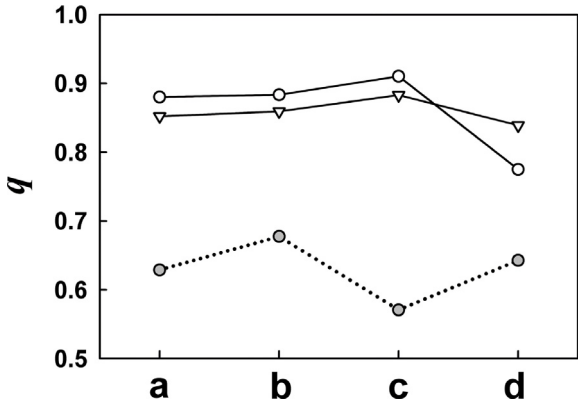

Fig. 9. Dependence of the efficiency q of spatial distribution. The open symbols represent the ABD system with bright B chromophores. The circles and downward triangles represent $k_{BD} = 0$ and $k_B D = 1$, respectively. The filled gray circles represent the AD system where all the B chromophores are replaced by D. Other detail of the parameters please see the main text of [95].
Source: Figure adapted with permission of [95].

tobacco mosaic virus coat protein monomers [96,97]. Their model is composed of three species of BChls, D, A and B. The BChls as sites of the model are uniformly distributed on each "disk", and the disks" are equally spaced. The difference between B and D sites is that the spectral overlap between B and A is larger than that between D and A. In other words, B serves as an energy "bridge" between D and A. The critical parameters in their model are the number ratio N_D/N_A, the transfer rate from D to A k_{DA}, and the dissipation rate k_S. Although a classical master equation from Förster theory was used to investigate the time evolution of the system in the theoretical description part, in which quantum dephasing and resonance are both neglected, there are also some useful conclusions in this article. For instance, the numerical calculation shows that an optimal number ratio exists when the transfer efficiency reaches its maximum under certain k_{DA} and k_S. The optimal values of N_D/N_A in their simulation depend positively on k_{DA}. When k_{DA} experiences a 100-fold increase, N_D/N_A rises from 5 to approximately 33, which may provide a theoretical interpretation for the scale difference of natural photosynthetic systems. The introduction of B sites opens up an alternative route to enhance energy transfer efficiency. The simulation of the AD model without B and the ABD model reveals that replacing some D sites with B can generally improve the transfer efficiency, and the evaluation of the spatial distribution would be completely reversed. Kim and Cao [95] created four different distributions of BChls illustrated in Figs. 8 and 9 shows the efficiency q. Notably, distribution (c) has the lowest q in AD systems while the highest q in the ABD system. The general features shared by photosynthetic complexes may be useful for constructing high-efficiency artificial photosynthetic systems.

Unlike the high-symmetry ring-shaped complexes, PSI and PSII in higher plants are more complicated in spatial configuration, and no complete theory has yet fully explained how the structural features in PSI and PSII support high-efficiency energy transfer. However, we can ask another question instead. What sets an optimal spatial structure apart from others, and what do optimal structures have in common? Following this question, Scholak et. al. [87,88] and Mostarda et. al. [98] tried to obtain the answer from a statistical perspective. They generated random spatial distributions of the BChls, with the number of BChls set to $N = 7$ in [87] and $N = 8$ in [98]. These values are similar to the number of pigments in the well-studied FMO complex in green sulfur bacteria. The transfer efficiency of the random complexes was then computed using the definition of efficiency η as

$$\eta(T) = \max_{t\in[0,T]} |\langle \text{out}|\psi(t)\rangle|^2, \tag{25}$$

where $|\psi(t)\rangle$ is the wave function of the system at time t, and T is the maximum time of simulation, which is set as $1/10$ of the time scale of direct interaction between the initial state and the final state to ensure the validity of the simulation results. The scale of the simulation is primarily restricted by computational cost, as the computation time scales exponentially with N, rendering simulations with $N \sim 100$ intractable.

The results and discussion in [87,98] share common ground but focus on different aspects. Their simulation results show that the conformations with high efficiency are rare but do exist among millions of stochastic ones. As a controlling indicator, the proportions of configurations with efficiency exceeding 90% are 0.005% and 0.015%, respectively. The spatial structure of a high-efficiency conformation is illustrated in Fig. 2(a) of [87] and its evolution of populations is shown in Fig. 2(b), where an almost-100% population of the output state is reached at time $\mathcal{T}'$. The spatial structure of this conformation is "asymmetric and non-periodic, hence far from trivial" [87]. However, no further discussion of this special structure is given in the remainder of this article. Mostarda et al. [98] went a step further on this issue. A network clusterization algorithm [99] was introduced to identify the geometric similarity of the high-efficiency configurations generated earlier. Finally, all the configurations are partitioned into three main classes called "pair", "inline" and "sparse", respectively. The differences among the three classes are broad, e.g., in their responses to small random displacements, i.e., the efficiency loss after

random displacement of the initial distribution (see Fig. 1b of [98]). The pair class shows its robustness against random displacement, whose average energy loss is around 0.06, compared with averages of 0.14 for the inline class and 0.10 for the sparse class. However, the cost of robustness is slower transfer time for the pair class. Next, we discuss the structural properties of the pair class, as a representation of all three classes, although their structural and dynamical behaviors are completely different. It is composed of two modules, the backbone (4 sites) and the pair (2 sites). The former is nearly in a straight line from the input site to the output site and approximately equally spaced, while the latter is very close spatially. Their dynamical characteristics are completely different. The pair is "inactive" with population on them never more than 0.075 in most of the time, while the backbone is quite "active" dynamically with populations always larger than 0.25. The inactive property of the pair indicates that it is a critical step of energy transfer, which is verified by the fact that removal of the pair results in an average efficiency loss of 0.2 and up to 0.32. Other classes, despite having entirely different configurations, exhibit similarly high efficiencies, suggesting that these diverse configurations also exist in natural photosynthetic systems and may even be found within a single complex as different pathways. Therefore, identifying these mechanisms in natural photosynthetic complexes and translating them into artificial photosynthetic systems remain promising directions for future study.

Note that studies reviewed above are all based on the perspective that the long-lived coherence is electronically originated, and the quantum mechanisms are induced by the specific spatial structure of the chromophores. However, there is also a different perspective that the long-lived coherence is vibronic in nature, so the long-lived electronic coherence may not be required to explain efficient photosynthetic EET [19,51,85,86,89]. As early as 2012, Christensson et al. [51] proposed a vibronic exciton Hamiltonian of FMO to explain the long-lived coherence. In this model, the vibrational modes of the chromophores are explicitly included in the system Hamiltonian rather than being treated as part of the environment. The result of numerical simulation of this model has shown a 1.3 ps dephasing time at 77 K, which is consistent with the experimental observation in [6]. The success of this model has indicated that the vibronic coupling may be the origin of the long-lived coherence in photosynthetic systems. In 2014, Fuller et al. [100] reported the 2D spectra of PSII reaction center using 2DES, where a series of oscillation frequencies were extracted from the spectrum. Moreover, they performed theoretical simulation of a special dimeric pair of PSII reaction center using the method developed by Butkus et al. [101,102] to distinguish the vibronic and electronic wavepacket motion. The reason of choosing this special pair is that it exhibits the strongest coupling and others couplings are much weaker. The simulation shows that coupling the dimer with a specific vibrational mode of 339 cm^{-1} could produce a coherence map that closely matches the experimental map (see Fig. 3(d)). Interestingly, the low-frequency mode 127 cm^{-1}, which exists in exciton frequency modes but not in vibrational modes, can also be produced by the electronic-vibrational coupling above. Their results shows the complexity of the spectra of photosynthetic complexes, where electronic, pure vibrational and mixed electron-vibrational (vibronic) coexist. The core question is that which one is in the majority? The subsequent works [85,86,103] further confirmed this viewpoint from different perspectives. Duan et al. [85],Thyrhaug et al. [103] repeated the photon echo 2D spectra experiment on FMO trimer of [6] at low temperature (77 K) and room temperature (296 K). In contrast to the earlier 277 K observations reported by Panitchayangkoon et al. [7], these spectra did not show clear evidence of long-lived electronic coherence. Further, Duan et al. [85] also analyzed the possible long-lived (~1 ps timescale) signal, argued that such signals could only be attributed to weak vibrational coherence. Maiuri et al. [86] addressed this question using a different experimental strategy. They used the mutagenesis-induced FMO mutant and its wild-type FMO to implement broadband pump–probe experiments, where the two mutant used in experiment exhibit significantly different electronic couplings compared to the wild-type FMO complex. If the signal observed in experiment originates from electronic coherence, the experiment result of mutant and wild-type must be noticeably different. However, the coherent oscillations and corresponding Fourier spectra of mutants and wild-type FMO observed in experiment were reported to be essentially consistent, which strongly indicated that the observed oscillation signals do not originate from electronic coherence. Although all these experiments were carried out on FMO complexes, considering the similarity of FMO with other complexes on distance between BChls, this perspective was supposed to be universal [85]. Overall, several lines of experimental evidence argue against assigning the observed long-lived oscillations solely to electronic coherence in natural photosynthetic complexes. Nevertheless, further experiments capable of disentangling electronic and vibronic contributions are needed to quantify their respective roles in EET and energy-transfer efficiency.

In the framework of vibronic coherence, some attempts of elucidating the mechanism of high-efficiency energy transfer has also been made. Malý et al. [104] proposed the role of vibronic states in energy transfer based on their numerical simulation on simplified models. Their study addressed the question of why low-energy states fail to trap energy and hinder energy transfer, in contrast to the behavior observed in semiconductors. The classical picture of vibronic state is the bath of electronic degree of freedom. In that picture, electronic excitation energy transferred into vibrational modes is usually treated as dissipation into molecular motion. However, Malý et al. [104] argued that the excitation of vibronic state led to a "transient hot bath" of the corresponding low-energy electronic state, which could be used by the excitation to escape the low-energy state. According to their simulation, the detrapping rate of excitation can be significantly increased when the vibrational mode is in resonance with the energy gap between the target state and the low-energy state. From this view, the low-energy state does not act as the trap during the lifetime of the corresponding vibronic state. A limitation of their simulations, however, is that the predicted escape probability under ideal conditions is only about 40%, which is relatively low and cannot directly account for the high efficiency of photosynthesis. Further theoretical and experimental work is needed to determine whether this mechanism operates in specific photosynthetic complexes and to quantify its contribution to EET.

As discussed in Sections 2.1 and 2.2, energy gradients and clustered pigment arrangements recur across many natural photosynthetic complexes. The mechanisms reviewed in Section 2.3 suggest that these structural features can modulate exciton delocalization, energy matching, and trapping. They therefore provide useful design motifs for artificial photosynthetic systems aimed at improving EET efficiency. The following section summarizes these design principles in more detail.

3. From natural to artificial design: Design principles and examples

Constructing an optimal artificial photosynthetic system is an important goal in the research of photosynthesis. To this end, we may gain inspiration from natural photosynthetic systems. It has been theoretically predicted and experimentally verified that quantum coherence and delocalized exciton states play a vital role in achieving the high EET efficiency observed in photosynthetic light-harvesting complexes [13]. However, it is still a topic of interest how these mechanisms can be exploited in the design of artificial photosynthetic systems. In this section, we review the design principles summarized from research on natural photosynthetic systems, and provide some discussion.

3.1. Design principles for bio-inspired photosynthetic systems

When constructing an artificial photosynthetic system, what we really care about are the parameters of the chromophores, i.e., the coordinates, dipole orientations, excitation energies, and interactions with the environment. Although this appears to be a well-defined optimization problem with a deterministic optimal solution, the high computational cost associated with solving the complex governing equations makes the use of standard optimization algorithms impractical. Rather than treating it as a conventional optimization problem, it is more constructive to interpret the factors that enhance EET efficiency as the fundamental design principles of photosynthetic systems. Such design principles have been discussed in a number of papers and reviews from distinct perspectives [13,18,22,27,65,105].

Ai et al. mainly focused on the geometric arrangements of chromophores. Through the calculation of a four-site model (see Scheme 1 of [22]), the following principles were suggested. The first is to establish an energy gradient from external sites to the target site, and the second is to form strongly-coupled clusters to create exciton delocalization and tune exciton energy for better energy matching between the donor and acceptor of each EET process. These principles paint a picture of natural photosynthetic systems as cluster-structured entities. The entire complex is constructed from strongly coupled chromophore clusters that are interconnected via weak couplings. In this respect, Bryant and Canniffe [106] noted that the dynamics of different coupling strengths should be treated by different theories, such as Förster theory for weak couplings and Redfield theory for strong couplings. Further, they analyzed the well-studied FMO complex and verified that it corresponds to the principles above.

The average inter-chromophore distance within clusters is a critical geometric parameter. As the dipole–dipole coupling strength, which governs chromophore interactions, scales as $1/r^6$, it exhibits a strong dependence on distance, increasing dramatically at short separations. However, this distance cannot be decreased indefinitely. Beyond a certain point, the benefits of stronger coupling are counteracted by detrimental effects such as exciton trapping or quenching [13,31,107], which leads to the shortening of the excitation lifetime. The opposing mechanisms indicate that an optimal spacing exists in natural systems. Ai et al. [22] investigated the population dynamics of site 4 in their model, $P_4(t)$, which is regarded as the target state in the EET process. By simulation of the model, it is found that $P_4(t)$ could be described as a double-exponential growth, with a rapid but minor rise and a major long-time exponential growth. To reflect the EET efficiency, the end-to-end effective transfer rate R_{eff} was defined as the component of the major exponent. Based on the coherent transfer theory, they proposed the analytical result of R_{eff}. Assuming that $|\varepsilon_k\rangle$ is the kth eigen state of the system Hamiltonian, and R_{mn} is the state-to-state EET rate, the analytical result R'_{eff} is written as

$$R'_{\text{eff}} \equiv \max\left\{\frac{R_{21}R_{32}}{R_{21}+R_{32}}, \frac{R_{32}R_{43}}{R_{32}+R_{43}}\right\}. \tag{26}$$

Fig. 10 displays the geometric dependence of R_{eff} by full non-Markovian quantum trajectory (NMQT) simulation and analytical result. As shown by a comparison of the two panels, the theoretical predictions agree well with the simulation results, which verifies that quantum coherence plays a crucial role in energy transfer. From the data presented in Fig. 10, the distance of chromophores in a cluster r exhibits an optimum at roughly 11 Å. This value is basically consistent with the situation of natural photosynthetic systems (~10 Å in many antenna complexes) [106] and can serve as an important guide for the design of artificial photosynthetic systems.

Beyond the arrangement of chromophores, it is also of considerable importance to exploit the vibrational spectral properties of the environment to enhance the EET process. Rey et al. [105] proposed a design principle named *the photon antenna mechanism*, which can coherently modify the sampling of environmental spectral noise to extract maximum noise strength and then accelerate the EET process. We illustrate the details of their proposal by a model taken from their article [105].

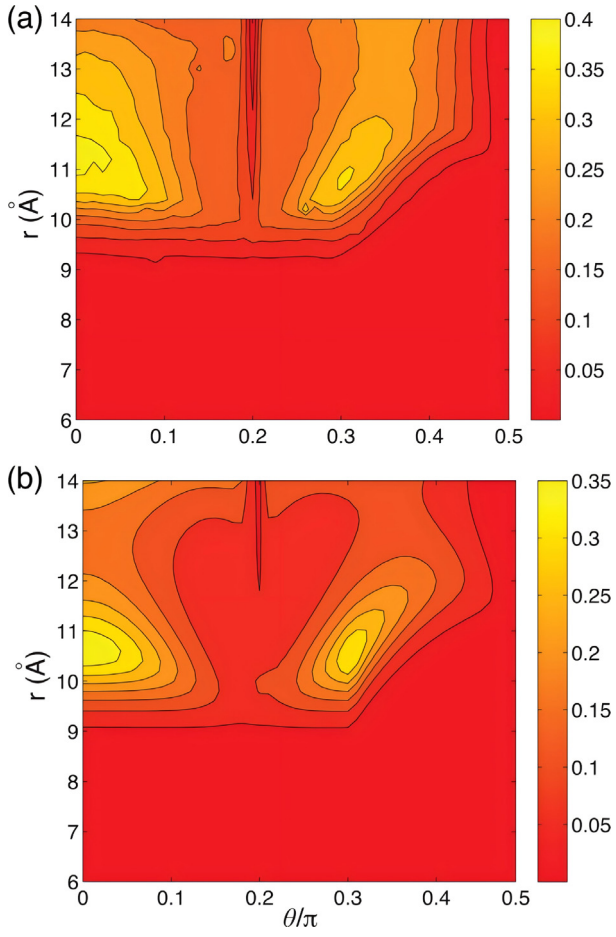

Fig. 10. Geometrical dependence of the effective transfer rate R_{eff} (ps^{-1}) as a function of the two geometrical parameters r and θ. (a) R_{eff} calculated from full CMRT-NMQT dynamical simulations. (b) R'_{eff} predicted by the analytical result in Eq. (26).
Source: Figure adapted with permission of [22].

Considering a light-harvesting antenna, which involves $N+1$ chromophores, the reaction center is labeled as 0 and the others are labeled sequentially from 1 to N. The electronic Hamiltonian of the system can be written as

$$H_S = \sum_i \varepsilon_i |i\rangle\langle i| + \sum_{i\neq j} J_{ij}|i\rangle\langle j| (i,j=0,1,2,\ldots,N), \tag{27}$$

where $|i\rangle$ and ε_i are the excited state and local energy of the ith chromophore (site), and J_{ij} is the coupling strength between the ith and jth sites. The delocalized exciton states $|e_n\rangle$ satisfying $H_S|e_n\rangle = e_n|e_n\rangle$ can be expressed in the site basis $|i\rangle$ as $|e_n\rangle = \sum_i C_{ni}|i\rangle$. The reaction center 0 is nearly isolated and can only be populated irreversibly from site N. To deal with the interaction between the system and the environment (i.e., the non-electronic degrees of freedom of chromophores and the protein scaffolds surrounding the chromophores), it is supposed that the system is coupled with a continuous bath of harmonic oscillators with environmental spectral density $J(\omega)$. According to the CMRT, it is appropriate to treat this problem in the exciton basis $\{|e_n\rangle\}$. The dynamics of the population $\rho_{nn}^{(S)}$ of the system is described as follows

$$\dot{\rho}_{mm}^{(S)} = \sum_{n\neq m} W_{mn}\rho_{nn}^{(S)} - \sum_{n\neq m}(W_{nm} + \Gamma_{e_m\to 0})\rho_{mm}^{(S)}, (m\neq 0)$$

$$\dot{\rho}_{00}^{(S)} = \sum_n \Gamma_{e_n \to 0} \rho_{nn}^{(S)}, \tag{28}$$

where the transition rates between eigen states $|e_m\rangle$ and $|e_n\rangle$ are

$$W_{mn} = \begin{cases} 2\pi J(E_{mn}) \chi_{mn} n(E_{mn}), & E_{mn} \geq 0 \\ 2\pi J(E_{mn}) \chi_{mn} [n(E_{mn}) + 1], & E_{mn} < 0 \end{cases} \tag{29}$$

with

$$\chi_{mn} = \sum_i |C_{mi} C_{ni}|^2, \tag{30}$$

$$n(\omega) = \frac{1}{\exp(\omega / k_B T) - 1}, \tag{31}$$

$$E_{mn} = E_m - E_n. \tag{32}$$

Eq. (29) indicates that the transition rates W_{mn} depend on the density of photons $n(\omega)$ and the spectral density $J(\omega)$ at a frequency equal to the energy gap E_{mn}. As has been noted by [106], the protein scaffolds of natural light-harvesting antennae can modify the parameters (e.g., the position and orientation of chromophores) to match the environment. Further, typical spectral densities of light-harvesting antenna complexes have at least one maximum at a finite frequency [108]. It is evident that natural photosynthetic systems can enhance their energy transfer rates by adjusting the geometric and energetic parameters of chromophores with protein scaffolds. This tuning aligns the energy gap with the maximum of the environmental spectral density, thereby optimizing performance under varying conditions. In artificial photosynthetic systems, similar attention should be given to replacing the protein scaffold with an engineered structure or other suitable support (see the introduction of semi-artificial photosynthetic systems in Section 3.2). We suggest that this represents a promising direction for future research.

3.2. Bio-inspired artificial photosynthetic systems

Artificial photosynthetic systems can be broadly classified into all-artificial and semi-artificial systems. All-artificial systems mimic selected functions of natural photosynthesis using entirely synthetic components, such as semiconductors, molecular photosensitizers, photocatalysts, or photoelectrochemical devices. These platforms are designed to absorb light, generate charge carriers, and drive reactions including hydrogen evolution, CO_2 reduction, and nitrogen fixation. Although they can provide efficient photon capture and charge separation, their product selectivity and capacity for multi-step synthesis of complex multi-carbon products are often limited.

Semi-artificial photosynthetic systems combine artificial light-harvesting or charge-separation components with biological modules derived from natural photosynthetic or metabolic systems. In such systems, selected functions of natural photosynthesis – for example, light absorption, electron delivery, or catalytic conversion – are replaced, supplemented, or coupled with synthetic materials, while enzymes or living cells retain their high selectivity, multistep catalytic capability, and potential for self-repair. This combination enables the tunable optical and electronic properties of nanomaterials, including light absorption, band structure, morphology, and interfacial charge transfer, to be integrated with biological catalysis [109,110]. For example, a self-assembled PCN-222–*E. coli* biohybrid uses a porphyrinic MOF as a light-capturing and photoelectron-donating component, while engineered cells use the resulting reducing power for hydrogen and lysine production [111].

To compare these two classes within a unified design framework, it is useful to proceed from simplified all-artificial assemblies to more integrated semi-artificial systems. All-artificial platforms offer well-defined and highly controllable architectures for isolating the effects of chromophore geometry, energetic ordering, molecular packing, and scaffold rigidity on excitation transport. These structure–function relationships then provide a basis for semi-artificial systems, in which similar design principles must operate together with interfacial electron transfer and biological or metabolic conversion. We therefore discuss fully artificial light-harvesting assemblies first and then examine how related principles appear in semi-artificial solar-to-chemical systems [109,110].

3.2.1. All-artificial systems

All-artificial light-harvesting platforms provide valuable model systems in which individual structural variables can be controlled directly. In particular, they make it possible to isolate the effects of chromophore position, donor–acceptor distance, energetic ordering, molecular packing, and scaffold rigidity before these variables are coupled to more complex catalytic or cellular processes.

A representative example is the DNA-origami antenna developed by Hemmig et al., in which donor dyes were arranged around a central acceptor with programmable nanoscale geometry [112]. By systematically varying donor number and donor–acceptor separation, this platform directly demonstrated how chromophore coordinates and antenna topology affect Förster-type energy transfer and the antenna effect. The ring-like donor arrangement surrounding a central acceptor further provides a simplified artificial analogue of the peripheral-antenna-to-reaction-center geometry found in purple-bacterial photosynthetic membranes. Such programmable DNA scaffolds therefore offer a controlled framework for testing the geometric design rules discussed in Section 3.1.

Energy-level ordering can be incorporated simultaneously with structural control. Han et al. constructed a bio-inspired sequential energy-transfer system by supramolecular copolymerization of three σ-platinated (hetero)acene chromophores [113]. The three components formed an energetically downhill visible-to-near-infrared cascade, enabling sequential transfer from the initial donor through an intermediate relay to the final acceptor. Dense and ordered chromophore packing supported long-range exciton migration, while the Pt(II)-containing molecular design reduced excessive stacking and aggregation-caused quenching. The resulting ternary copolymer achieved an overall sequential energy-transfer efficiency of 87.4%, illustrating that an effective artificial energy funnel requires both energetic matching and packing geometries that impart directionality to exciton transport and preserve useful excited-state populations.

Structural order can also control exciton transport. Haldar et al. used a surface-anchored metal–organic framework to assemble donor and acceptor chromophores in a highly ordered crystalline architecture [114]. By introducing energy-accepting linkers at defined positions, they observed strongly anisotropic transport of an excimer-related excited state along a crystallographic direction. This result shows that short-range chromophore packing and long-range mesoscale order can jointly define the pathway and direction of exciton migration. Such ordered frameworks are therefore promising scaffolds for constructing artificial antenna networks that funnel excitation toward spatially defined reaction centers.

Mu et al. [115] further demonstrated that strong intra-cluster coupling must be balanced against aggregation-induced loss channels. Their purple-bacteria-inspired polymeric supramolecular columns used stacked donor chromophores to support exciton diffusion along the column, while acceptor molecules were intercalated within the assembly. The slightly twisted donor geometry preserved fluorescence by limiting overly tight π–π overlap, thereby enabling detectable energy transfer even at a donor–acceptor ratio of 20,000:1 and an antenna effect exceeding 100. This example captures the trade-off discussed in Section 3.1, since dense packing can promote electronic coupling and exciton diffusion, whereas local geometry must limit concentration quenching.

3.2.2. Semi-artificial systems

The all-artificial platforms discussed above clarify how energy gradients, chromophore geometry, and scaffold organization influence excitation transport. Semi-artificial systems extend these principles to solar-to-chemical conversion by integrating synthetic light-harvesting or charge-separation components with biological modules, such as isolated enzymes, photosynthetic proteins, or living cells. In addition to intramolecular and interchromophore energy transfer, their design must account for material morphology, surface charge, band alignment, redox mediators, and the spatial organization of the bio–abiotic interface [109,110].

At the molecular level, semi-artificial systems can retain natural photochemical reaction centers while extending their light-harvesting functions with synthetic absorbers. Amoruso et al. [116] constructed quantum-dot–RC–LH1 nanoconjugates in which excitation energy was transferred from a synthetic quantum-dot antenna to purple-bacterial reaction-center–light-harvesting-1 complexes through Förster resonance energy transfer. This system provides a direct semi-artificial analogue of the donor–acceptor geometry principles discussed above, because spectral overlap, interfacial separation, and attachment geometry together determine whether captured excitation can be transferred productively to the native photochemical core. Liu et al. [117] further developed genetically encoded pigment–protein chimeras in which plant light-harvesting complexes were covalently linked to purple-bacterial reaction centers, enabling polychromatic light harvesting through the combination of complementary pigment systems. These studies demonstrate that engineered protein interfaces can regulate energy matching and antenna–reaction-center connectivity while preserving the charge-separation function of natural reaction centers.

Semi-artificial design can also couple synthetic light absorbers to cellular metabolism. In the self-assembled PCN-222–*E. coli* biohybrid reported by Li et al. [111], the porphyrinic MOF PCN-222 functions as a light-harvesting and photoelectron-donating component, whereas engineered *E. coli* provides the metabolic machinery for fuel and chemical production. The rod-like MOF morphology promotes bacterial adhesion, and its visible-light absorption and electronic structure enable photogenerated electrons to enter the cellular redox network. Riboflavin was proposed to mediate interfacial electron transfer, while secreted small organic acids assist hole consumption. Under illumination, the hybrid increased intracellular NADPH availability, supported hydrogen production, and enhanced lysine production relative to the bacterial control [111].

This example illustrates how the principles summarized in Section 3.1 can be extended beyond artificial antenna design. Energy-level alignment provides a thermodynamic driving force for electron transfer; interfacial proximity and surface organization regulate coupling between the material and the cell; and the local chemical environment, including mediators and hole scavengers, determines whether charge separation is converted into useful reducing power rather than recombination or photodamage. Semi-artificial photosynthesis therefore requires coordinated structural design across light absorption, charge transport, interfacial electron transfer, and metabolic utilization.

The same design logic applies at larger length scales. Song et al. [118] introduced Ru single-atom bridges at the interface between porous carbon nitride and *Shewanella*, where the interfacial $Ru-N_4$ structure promoted charge separation, lowered the electron-transfer barrier, and enhanced direct electron uptake by the microorganism. This study highlights how atomically defined interfacial coordination can improve electronic coupling across a bio–abiotic junction. Likewise, Chen et al. [119] combined semiconductor components with purple-membrane-derived vesicles to construct a semi-artificial platform for CO_2 reduction. Together, these examples show that energy-level alignment, interfacial distance, local chemical environment, and downstream catalytic trapping must be optimized as a continuous energy-flow process rather than as isolated design variables.

Overall, semi-artificial systems connect the structural principles identified in all-artificial antenna assemblies with the catalytic selectivity and metabolic versatility of biological modules. Their future development will require the integrated optimization of antenna architecture, charge-separation pathways, bio–abiotic interfacial coupling, and catalytic or metabolic turnover, so that solar-energy capture and chemical conversion can be designed as a single functional network [109,110].

4. Conclusion and future outlook

This review has examined the relationship between molecular architecture and quantum effects in oxygenic and anoxygenic phototrophs. Across PSI–LHCI, PSII–SC, LH2–LH1–RC, and FMO, excitation-energy transfer is governed by the coupled effects of pigment geometry, intermolecular distance and orientation, electronic coupling, site-energy organization, protein–environment interactions, and reaction-center trapping. These factors do not act independently. Instead, they collectively determine whether excitation transport proceeds through partially delocalized dynamics, incoherent hopping, or a mixed regime, and whether the resulting excitation is productively converted into charge separation.

The comparison of natural photosynthetic systems indicates that high performance cannot be attributed to a single structural motif or to quantum coherence alone. PSI combines a densely connected pigment network with protein-tuned low-energy states that favor rapid equilibration and trapping, whereas PSII employs a more heterogeneous antenna-to-core topology that balances excitation migration, photoprotection, and charge separation. Similarly, ring-based LH2–LH1 architectures emphasize strong local coupling and collective excitonic states, while FMO illustrates the importance of a protein-shaped site-energy landscape with defined input and output regions. Quantum coherence should therefore be regarded as a system-dependent dynamical feature that may contribute to excitation transport under appropriate structural and environmental conditions, rather than as a universal and independent origin of high efficiency [13,19,24].

The structural principles identified in natural photosynthesis provide a useful basis for artificial light-energy conversion. All-artificial assemblies enable controlled examination of chromophore placement, donor–acceptor geometry, energetic cascades, molecular packing, and scaffold rigidity. Semi-artificial systems further integrate these principles with natural reaction centers, enzymes, or living cells, thereby extending energy transport to interfacial electron transfer and chemical or metabolic conversion. In such systems, efficient excitation transfer alone is insufficient; energy-level alignment, interfacial coupling, redox mediation, catalytic trapping, product selectivity, and long-term stability must be optimized as parts of a continuous energy-flow network [109,110].

Several issues need to be addressed before these structural principles can be translated reliably into artificial systems. First, improved integration of high-resolution structural methods, ultrafast spectroscopy, and quantitative kinetic measurements is required to establish how pigment geometry, energetic disorder, and environmental fluctuations jointly control transfer pathways in intact complexes and biohybrid systems. Second, multiscale theoretical approaches should connect atomistic structures with experimentally constrained electronic couplings, site energies, spectral densities, charge-separation kinetics, and competing loss channels. The applicability of Förster, Redfield-type, CMRT, and HEOM-based descriptions should be evaluated according to the relevant coupling, disorder, and environmental regimes rather than treated as interchangeable methods.

By integrating quantum–mechanical theory, structural biology, spectroscopy, and materials engineering, future research can clarify how natural architectures balance energy transport with robustness and photoprotection. Such knowledge will support the rational design of artificial and semi-artificial systems in which light absorption, excitation or charge transport, interfacial electron transfer, and chemical conversion are optimized as a unified functional process.

CRediT authorship contribution statement

Kai-Ya Zhang: Writing – review & editing, Writing – original draft. **Rui Li:** Writing – original draft. **Yi Li:** Writing – review & editing. **Ming-Zi Jin:** Writing – review & editing. **Rong-Hang Chen:** Writing – review & editing, Supervision. **Qing Ai:** Writing – review & editing, Supervision, Project administration.

Declaration of competing interest

The authors declare that they have no known competing financial interests or personal relationships that could have appeared to influence the work reported in this paper.

Acknowledgments

This work is supported by the National Natural Science Foundation of China under Grant no. 62461160263, Innovation Program for Quantum Science and Technology under Grant no. 2023ZD0300200, and Guangdong Provincial Quantum Science Strategic Initiative under Grant no. GDZX2505004.

References

[1] T. Mirkovic, G.D. Scholes, Photosynthetic light harvesting, in: L. Björn (Ed.), Photobiology, Springer, New York, NY, 2015, pp. 365–392, http://dx.doi.org/10.1007/978-1-4939-1468-5_17.

[2] Y. Dubi, Interplay between dephasing and geometry and directed heat flow in exciton transfer complexes, J. Phys. Chem. C (ISSN: 1932-7447) 119 (45) (2015) 25252–25259, http://dx.doi.org/10.1021/acs.jpcc.5b08493.

[3] J. Barber, Photosystem II: a multisubunit membrane protein that oxidises water, Curr. Opin. Struct. Biol. 12 (4) (2002) 523–530, http://dx.doi.org/10.1016/s0959-440x(02)00357-3, URL: https://www.sciencedirect.com/science/article/abs/pii/S0959440X02003573.

[4] Y. Mazor, H. Toporik, N. Nelson, Temperature-sensitive PSII and promiscuous PSI as a possible solution for sustainable photosynthetic hydrogen production, Biochim. Biophys. Acta Bioenerg. 1817 (7) (2012) 1122–1126, http://dx.doi.org/10.1016/j.bbabio.2012.01.005, URL: https://www.sciencedirect.com/science/article/pii/S0005272812000072.

[5] H. Toporik, I. Carmeli, I. Volotsenko, M. Molotskii, Y. Rosenwaks, C. Carmeli, N. Nelson, Large photovoltage generated by plant photosystem I crystals, Adv. Mater. 24 (22) (2012) 2988–2991, http://dx.doi.org/10.1002/adma.201200039, URL: https://advanced.onlinelibrary.wiley.com/doi/abs/10.1002/adma.201200039.

[6] G.-S. Engel, T.-R. Calhoun, E.-L. Read, T.-K. Ahn, T. Mancal, Y.-C. Cheng, R.-E. Blankenship, G.-R. Fleming, Evidence for wavelike energy transfer through quantum coherence in photosynthetic systems, Nature 446 (7137) (2007) 782–786, http://dx.doi.org/10.1038/nature05678, URL: https://www.nature.com/articles/nature05678.

[7] G. Panitchayangkoon, D. Hayes, K.-A. Fransted, J.-R. Caram, E. Harel, J.-Z. Wen, R.-E. Blankenship, G.-S. Engel, Long-lived quantum coherence in photosynthetic complexes at physiological temperature, Proc. Natl. Acad. Sci. USA 107 (29) (2010) 12766–12770, http://dx.doi.org/10.1073/pnas.1005484107, URL: https://www.pnas.org/doi/full/10.1073/pnas.1005484107.

[8] E. Collini, C.-Y. Wong, K.-E. Wilk, P.-M.-G. Curmi, P. Brumer, G.-D. Scholes, Coherently wired light-harvesting in photosynthetic marine algae at ambient temperature, Nature 463 (7281) (2010) 644–U69, http://dx.doi.org/10.1038/nature08811, URL: https://www.nature.com/articles/nature08811.

[9] F. Fassioli, R. Dinshaw, P.C. Arpin, G.D. Scholes, Photosynthetic light harvesting: excitons and coherence, J. R. Soc. Interface 11 (2014) 20130901, http://dx.doi.org/10.1098/rsif.2013.0901.

[10] T.B. Arp, J. Kistner-Morris, V. Aji, R.J. Cogdell, R. van Grondelle, N.M. Gabor, Quieting a noisy antenna reproduces photosynthetic light-harvesting spectra, Science 368 (6498) (2020) 1490–1495, http://dx.doi.org/10.1126/science.aba6630, URL: https://www.science.org/doi/10.1126/science.aba6630.

[11] J. Struempfer, M. Sener, K. Schulten, How quantum coherence assists photosynthetic light-harvesting, J. Phys. Chem. Lett. 3 (4) (2012) 536–542, http://dx.doi.org/10.1021/jz201459c, URL: https://pubs.acs.org/doi/10.1021/jz201459c.

[12] R. Hildner, D. Brinks, J.-B. Nieder, R.-J. Cogdell, N.F. van Hulst, Quantum coherent energy transfer over varying pathways in single light-harvesting complexes, Science 340 (6139) (2013) 1448–1451, http://dx.doi.org/10.1126/science.1235820, URL: https://www.science.org/doi/10.1126/science.1235820.

[13] T. Mirkovic, E.-E. Ostroumov, J.-M. Anna, R. van Grondelle, Govindjee, G.-D. Scholes, Light absorption and energy transfer in the antenna complexes of photosynthetic organisms, Chem. Rev. 117 (2) (2017) 249–293, http://dx.doi.org/10.1021/acs.chemrev.6b00002.

[14] A. Jha, F. Zheng, Z. Liu, S. Mukamel, M. Thorwart, R.J.D. Miller, H.-G. Duan, Quantum coherent dynamics in photosynthetic protein complexes, Chem. Soc. Rev. 55 (2026) 1089–1130, http://dx.doi.org/10.1039/D5CS00948K.

[15] H. Lee, Y.-C. Cheng, G.R. Fleming, Coherence dynamics in photosynthesis: Protein protection of excitonic coherence, Science 316 (5830) (2007) 1462–1465, http://dx.doi.org/10.1126/science.1142188.

[16] E. Romero, R. Augulis, V. Novoderezhkin, M. Ferretti, J. Thieme, D. Zigmantas, R. van Grondelle, Quantum coherence in photosynthesis for efficient solar-energy conversion, Nat. Phys. 10 (2014) 676–682, http://dx.doi.org/10.1038/nphys3017.

[17] G.-D. Scholes, G.-R. Fleming, L.-X. Chen, A. Aspuru-Guzik, A. Buchleitner, D.-F. Coker, G.-S. Engel, R. van Grondelle, A. Ishizaki, D.-M. Jonas, J.-S. Lundeen, J.-K. McCusker, S. Mukamel, J.-P. Ogilvie, A. Olaya-Castro, M.-A. Ratner, F.-C. Spano, K.-B. Whaley, X.-Y. Zhu, Using coherence to enhance function in chemical and biophysical systems, Nature 543 (7647) (2017) 647–656, http://dx.doi.org/10.1038/nature21425, URL: https://www.nature.com/articles/nature21425.

[18] E. Romero, V.-I. Novoderezhkin, R. van Grondelle, Quantum design of photosynthesis for bio-inspired solar-energy conversion, Nature 543 (7645) (2017) 355–365, http://dx.doi.org/10.1038/nature22012, URL: https://www.nature.com/articles/nature22012.

[19] J.-S. Cao, R.-J. Cogdell, D.F. Coker, H.-G. Duan, J. Hauer, U. Kleinekathoefer, T.-L.-C. Jansen, T. Mancal, R.-J.D. Miller, J.-P. Ogilvie, V. Prokhorenko, T. Renger, H.-S. Tan, R. Tempelaar, M. Thorwart, E. Thyrhaug, S. Westenhoff, D. Zigmantas, Quantum biology revisited, Sci. Adv. 6 (14) (2020) http://dx.doi.org/10.1126/sciadv.aaz4888, URL: https://www.science.org/doi/10.1126/sciadv.aaz4888.

[20] R. Croce, H. van Amerongen, Light harvesting in oxygenic photosynthesis: Structural biology meets spectroscopy, Science 369 (6506) (2020) eaay2058, http://dx.doi.org/10.1126/science.aay2058.

[21] R. Dods, P. Bath, D. Morozov, V.-A. Gagner, D. Arnlund, H.-L. Luk, J. Kubel, M. Maj, A. Vallejos, C. Wickstrand, R. Bosman, K.-R. Beyerlein, G. Nelson, M. Liang, D. Milathianaki, J. Robinson, R. Harimoorthy, P. Berntsen, E. Malmerberg, L. Johansson, R. Andersson, S. Carbajo, E. Claesson, C.-E. Conrad, P. Dahl, G. Hammarin, M.-S. Hunter, C. Li, S. Lisova, A. Royant, C. Safari, A. Sharma, G.-J. Williams, O. Yefanov, S. Westenhoff, J. Davidsson, D.-P. DePonte, S. Boutet, A. Barty, G. Katona, G. Groenhof, G. Branden, R. Neutze, Ultrafast structural changes within a photosynthetic reaction centre, Nature 589 (7841) (2021) 310+, http://dx.doi.org/10.1038/s41586-020-3000-7.

[22] Q. Ai, T.-C. Yen, B.-Y. Jin, Y.-C. Cheng, Clustered geometries exploiting quantum coherence effects for efficient energy transfer in light harvesting, J. Phys. Chem. Lett. 4 (15) (2013) 2577–2584, http://dx.doi.org/10.1021/jz4011477.

[23] R.E. Blankenship, Molecular Mechanisms of Photosynthesis, second ed., Wiley-Blackwell, Oxford, UK, 2014, p. 72, http://dx.doi.org/10.1002/9781118658613.

[24] A. Chenu, G.-D. Scholes, Coherence in energy transfer and photosynthesis, Annu. Rev. Phys. Chem. 66 (1) (2015) 69–96, http://dx.doi.org/10.1146/annurev-physchem-040214-121713, URL: https://www.annualreviews.org/content/journals/10.1146/annurev-physchem-040214-121713.

[25] P. Akhtar, I. Caspy, P.J. Nowakowski, T. Malavath, N. Nelson, H.-S. Tan, P.H. Lambrev, Two-dimensional electronic spectroscopy of a minimal photosystem i complex reveals the rate of primary charge separation, J. Am. Chem. Soc. (ISSN: 0002-7863) 143 (36) (2021) 14601–14612, http://dx.doi.org/10.1021/jacs.1c05010, URL: https://pubs.acs.org/doi/10.1021/jacs.1c05010.

[26] E. Kim, D. Lee, S. Sakamoto, J.-Y. Jo, M. Vargas, A. Ishizaki, J. Minagawa, H. Kim, Network analysis with quantum dynamics clarifies why photosystem II exploits both chlorophyll a and b, Sci. Adv. 11 (2025) eads0327, http://dx.doi.org/10.1126/sciadv.ads0327.

[27] A. Mattioni, F. Caycedo-Soler, S.F. Huelga, M.B. Plenio, Design principles for long-range energy transfer at room temperature, Phys. Rev. X 11 (2021) 041003, http://dx.doi.org/10.1103/PhysRevX.11.041003.

[28] J. Adolphs, T. Renger, How proteins trigger excitation energy transfer in the FMO complex of green sulfur bacteria, Biophys. J. (ISSN: 1542-0086) 91 (8) (2006) 2778–2797, http://dx.doi.org/10.1529/biophysj.105.079483.

[29] A. Ishizaki, G.R. Fleming, Theoretical examination of quantum coherence in a photosynthetic system at physiological temperature, Proc. Natl. Acad. Sci. USA (ISSN: 0027-8424) 106 (41) (2009) 17255–17260, http://dx.doi.org/10.1073/pnas.0908989106.

[30] N. Nelson, Plant photosystem I–the most efficient nano-photochemical machine, J. Nanosci. Nanotechnol. 9 (3) (2009) 1709–1713, http://dx.doi.org/10.1166/jnn.2009.si01.

[31] R. Croce, H. van Amerongen, Light-harvesting in photosystem i, Photosynth. Res. 116 (2-3, SI) (2013) 153–166, http://dx.doi.org/10.1007/s11120-013-9838-x.
[32] E. Wientjes, G.T. Oostergetel, S. Jansson, E.J. Boekema, R. Croce, The role of Lhca complexes in the supramolecular organization of higher plant photosystem i, J. Biol. Chem. 284 (12) (2009) 7803–7810, http://dx.doi.org/10.1074/jbc.M808395200.
[33] E. Wientjes, R. Croce, The light-harvesting complexes of higher-plant photosystem I: Lhca1/4 and Lhca2/3 form two red-emitting heterodimers, Biochem. J. (ISSN: 0264-6021) 433 (3) (2011) 477–485, http://dx.doi.org/10.1042/BJ20101538.
[34] R.C. Jennings, G. Zucchelli, R. Croce, F.M. Garlaschi, The photochemical trapping rate from red spectral states in PSI-LHCI is determined by thermal activation of energy transfer to bulk chlorophylls, Biochim. Biophys. Acta Bioenerg. 1557 (1–3) (2003) 91–98, http://dx.doi.org/10.1016/S0005-2728(02)00399-7.
[35] E. Wientjes, I. van.Stokkum, H. van.Amerongen, R. Croce, The role of the individual lhcas in photosystem I excitation energy trapping, Biophys. J. (ISSN: 0006-3495) 101 (3) (2011) 745–754, http://dx.doi.org/10.1016/j.bpj.2011.06.045, URL: https://www.sciencedirect.com/science/article/pii/S0006349511007752.
[36] G.S. Beddard, G. Porter, Concentration quenching in chlorophyll, Nature 260 (1976) 366–367, http://dx.doi.org/10.1038/260366a0.
[37] F. Müh, A. Zouni, Structural basis of light-harvesting in the photosystem II core complex, Protein Sci. 29 (2020) 1090–1119, http://dx.doi.org/10.1002/pro.3841.
[38] E.G. Andrizhiyevskaya, D. Frolov, R. van Grondelle, J.P. Dekker, On the role of the CP47 core antenna in the energy transfer and trapping dynamics of photosystem II, Phys. Chem. Chem. Phys. 6 (2004) 4810–4819, http://dx.doi.org/10.1039/b411977k.
[39] H. van Amerongen, R. Croce, Light harvesting in photosystem II, Photosynth. Res. 116 (2013) 251–263, http://dx.doi.org/10.1007/s11120-013-9824-3.
[40] X. Wei, X. Su, P. Cao, X. Liu, W. Chang, M. Li, X. Zhang, Z. Liu, Structure of spinach photosystem II-LHCII supercomplex at 3.2 a resolution, Nature 534 (2016) 69–74.
[41] X. Su, J. Ma, X. Wei, P. Cao, D. Wang, C. Gao, R. Wang, S.F. Sui, X. Zhang, Z. Liu, Structure and assembly mechanism of plant C2s2m2-type PSII-lhcii supercomplex, Science 357 (2017) 815–820.
[42] S.-J. Yang, E.A. Arsenault, K. Orcutt, M. Iwai, Y. Yoneda, G.R. Fleming, From antenna to reaction center: Pathways of ultrafast energy and charge transfer in photosystem II, Proc. Natl. Acad. Sci. USA 119 (42) (2022) e2208033119, http://dx.doi.org/10.1073/pnas.2208033119.
[43] Y. Shibata, S. Nishi, K. Kawakami, J.-R. Shen, T. Renger, Photosystem II does not possess a simple excitation energy funnel: time-resolved fluorescence spectroscopy meets theory, J. Am. Chem. Soc. (ISSN: 0002-7863) 135 (18) (2013) 6903–6914, http://dx.doi.org/10.1021/ja312586p.
[44] J.-J.-J. Roden, D.-I.-G. Bennett, K.-B. Whaley, Long-range energy transport in photosystem II, J. Chem. Phys. 144 (24) (2016) 245101, http://dx.doi.org/10.1063/1.4953243.
[45] S.-J. Yang, D.J. Wales, E.J. Woods, G.R. Fleming, Design principles for energy transfer in the photosystem II supercomplex from kinetic transition networks, Nat. Commun. 15 (2024) 8763, http://dx.doi.org/10.1038/s41467-024-53138-z.
[46] R.E. Fenna, B.W. Matthews, Chlorophyll arrangement in a bacteriochlorophyll protein from Chlorobium limicola, Nature (ISSN: 0028-0836) 258 (5536) (1975) 573–577, http://dx.doi.org/10.1038/258573a0.
[47] D.E. Tronrud, J. Wen, L. Gay, R.E. Blankenship, The structural basis for the difference in absorbance spectra for the FMO antenna protein from various green sulfur bacteria, Photosynth. Res. 100 (2) (2009) 79–87, http://dx.doi.org/10.1007/s11120-009-9430-6.
[48] M. Schmidt am Busch, F. Müh, M. El-Amine Madjet, T. Renger, The eighth bacteriochlorophyll completes the excitation energy funnel in the FMO protein, J. Phys. Chem. Lett. 2 (2) (2011) 93–98, http://dx.doi.org/10.1021/jz101541b.
[49] J. Moix, J. Wu, P. Huo, D. Coker, J. Cao, Efficient energy transfer in light-harvesting systems, III: The influence of the eighth bacteriochlorophyll on the dynamics and efficiency in FMO, J. Phys. Chem. Lett. 2 (24) (2011) 3045–3052, http://dx.doi.org/10.1021/jz201259v.
[50] P. Rebentrost, M. Mohseni, I. Kassal, S. Lloyd, A. Aspuru-Guzik, Environment-assisted quantum transport, New J. Phys. 11 (2009) http://dx.doi.org/10.1088/1367-2630/11/3/033003, URL: https://iopscience.iop.org/article/10.1088/1367-2630/11/3/033003.
[51] N. Christensson, H.-F. Kauffmann, T. Pullerits, T. Mancal, Origin of long-lived coherences in light-harvesting complexes, J. Phys. Chem. B 116 (25) (2012) 7449–7454, http://dx.doi.org/10.1021/jp304649c, URL: https://pubs.acs.org/doi/pdf/10.1021/jp304649c.
[52] A. Ishizaki, G.-R. Fleming, Unified treatment of quantum coherent and incoherent hopping dynamics in electronic energy transfer: Reduced hierarchy equation approach, J. Chem. Phys. 130 (23) (2009) 234111, http://dx.doi.org/10.1063/1.3155372, URL: https://pubs.aip.org/aip/jcp/article/130/23/234111/924993/Unified-treatment-of-quantum-coherent-and-incoherent.
[53] Y.-H. Hwang-Fu, W. Chen, Y.-C. Cheng, A coherent modified Redfield theory for excitation energy transfer in molecular aggregates, Chem. Phys. (ISSN: 0301-0104) 447 (2015) 46–53, http://dx.doi.org/10.1016/j.chemphys.2014.11.026, URL: https://www.sciencedirect.com/science/article/pii/S0301010414003358.
[54] S.I.E. Vulto, M.A. de Baat, R.J.W. Louwe, H.P. Permentier, T. Neef, M. Miller, H. van Amerongen, T.J. Aartsma, Exciton simulations of optical spectra of the FMO complex from the green sulfur bacterium chlorobium tepidum at 6 k, J. Phys. Chem. B 102 (47) (1998) 9577–9582, http://dx.doi.org/10.1021/jp982095l.
[55] R.J. Cogdell, A. Gall, J. Köhler, The architecture and function of the light-harvesting apparatus of purple bacteria: from single molecules to in vivo membranes, Q. Rev. Biophys. 39 (3) (2006) 227–324, http://dx.doi.org/10.1017/S0033583506004434.
[56] K. Mukai, S. Abe, H. Sumi, Theory of rapid excitation-energy transfer from B800 to optically forbidden exciton states of B850 in the antenna system LH2 of photosynthetic purple bacteria, J. Phys. Chem. B (ISSN: 1520-6106) 103 (29) (1999) 6096–6102, http://dx.doi.org/10.1021/jp984469g.
[57] S. Yang, D.-Z. Xu, Z. Song, C.-P. Sun, Dimerization-assisted energy transport in light-harvesting complexes, J. Chem. Phys. 132 (23) (2010) 234501, http://dx.doi.org/10.1063/1.3435213, URL: https://pubs.aip.org/aip/jcp/article/132/23/234501/71823/Dimerization-assisted-energy-transport-in-light.
[58] Y. Cheng, R. Silbey, Coherence in the B800 ring of purple bacteria LH2 - art. no. 028103, Phys. Rev. Lett. 96 (2) (2006) http://dx.doi.org/10.1103/PhysRevLett.96.028103.
[59] H. Oka, Role of an elliptical structure in photosynthetic energy transfer: Collaboration between quantum entanglement and thermal fluctuation, Sci. Rep. 6 (2016) 26058, http://dx.doi.org/10.1038/srep26058.
[60] D. Wang, O.-C. Fiebig, D. Harris, H. Toporik, Y. Ji, C. Chuang, M. Nairat, A.-L. Tong, J.-I. Ogren, S.-M. Hart, J. Cao, J.-N. Sturgis, Y. Mazor, G.-S. Schlau-Cohen, Elucidating interprotein energy transfer dynamics within the antenna network from purple bacteria, Proc. Natl. Acad. Sci. USA 120 (28) (2023) e2220477120, http://dx.doi.org/10.1073/pnas.2220477120, URL: https://www.pnas.org/doi/10.1073/pnas.2220477120.
[61] Q. Shi, L.-P. Chen, G.-J. Nan, R.-X. Xu, Y.-J. Yan, Efficient hierarchical Liouville space propagator to quantum dissipative dynamics, J. Chem. Phys. 130 (8) (2009) 084105, http://dx.doi.org/10.1063/1.3077918.
[62] Y. Tanimura, R. Kubo, Time evolution of a quantum system in contact with a nearly gaussian-markoffian noise bath, J. Phys. Soc. Japan 58 (1) (1989) 101–114, http://dx.doi.org/10.1143/JPSJ.58.101, URL: https://journals.jps.jp/doi/10.1143/JPSJ.58.101.
[63] M.-J. Tao, N.-N. Zhang, P.-Y. Wen, F.-G. Deng, Q. Ai, G.-L. Long, Coherent and incoherent theories for photosynthetic energy transfer, Sci. Bull. (ISSN: 2095-9273) 65 (4) (2020) 318–328, http://dx.doi.org/10.1016/j.scib.2019.12.009, URL: https://www.sciencedirect.com/science/article/pii/S2095927319307078.
[64] T. Renger, Theory of excitation energy transfer: from structure to function, Photosynth. Res. 102 (2-3, SI) (2009) 471–485, http://dx.doi.org/10.1007/s11120-009-9472-9.
[65] J.-S. Cao, R.-J. Silbey, Optimization of exciton trapping in energy transfer processes, J. Phys. Chem. A 113 (50) (2009) 13825–13838, http://dx.doi.org/10.1021/jp9032589, URL: https://pubs.acs.org/doi/pdf/10.1021/jp9032589.
[66] R.E. Blankenship, Molecular Mechanisms of Photosynthesis, third ed., Wiley, 2021.
[67] R.E. Blankenship, D.M. Tiede, J. Barber, G.W. Brudvig, G. Fleming, M. Ghirardi, M.R. Gunner, W. Junge, D.M. Kramer, A. Melis, T.A. Moore, C.C. Moser, D.G. Nocera, A.J. Nozik, D.R. Ort, W.W. Parson, R.C. Prince, R.T. Sayre, Comparing photosynthetic and photovoltaic efficiencies and recognizing the potential for improvement, Science 332 (6031) (2011) 805–809, http://dx.doi.org/10.1126/science.1200165.
[68] Govindjee, R. Govindjee, Primary events in photosynthesis, Sci. Am. 231 (1974) 68–82.
[69] H. van Amerongen, L. Valkunas, R. van Grondelle, Photosynthetic Excitons, World Scientific Publishing, Singapore, 2000.
[70] N. Nelson, W. Junge, Structure and energy transfer in photosystems of oxygenic photosynthesis, in: R. Kornberg (Ed.), Annu. Rev. Biochem., in: Annual Review of Biochemistry, vol. 84, 2015, pp. 659–683, http://dx.doi.org/10.1146/annurev-biochem-092914-041942.
[71] N.V. Karapetyan, A.R. Holzwarth, M. Rögner, The photosystem I trimer of cyanobacteria: molecular organization, excitation dynamics and physiological significance, FEBS Lett. (ISSN: 0014-5793) 460 (3) (1999) 395–400, http://dx.doi.org/10.1016/S0014-5793(99)01352-6, URL: https://www.sciencedirect.com/science/article/pii/S0014579399013526.

[72] M. Brecht, V. Radics, J.B. Nieder, R. Bittl, Protein dynamics-induced variation of excitation energy transfer pathways, Proc. Natl. Acad. Sci. USA 106 (29) (2009) 11857–11861, http://dx.doi.org/10.1073/pnas.0903586106, URL: https://www.pnas.org/doi/abs/10.1073/pnas.0903586106.

[73] Y. Yoneda, E. Arsenault, S. Yang, J. Strumpfer, K. Schulten, The initial charge separation step in oxygenic photosynthesis, Nat. Commun. 13 (2022) 2275, http://dx.doi.org/10.1038/s41467-022-29983-1.

[74] Y.-C. Yang, J.-C. Hong, J. Wang, Coarse-graining kinetic networks in photosynthetic energy transport, J. Chin. Chem. Soc. (ISSN: 0009-4536) 70 (10) (2023) 1864–1878, http://dx.doi.org/10.1002/jccs.202300290.

[75] Y.-Z. Zhang, K. Li, B.-Y. Qin, J.-P. Guo, Q.-B. Zhang, D.-L. Zhao, X.-L. Chen, J. Gao, L.-N. Liu, L.-S. Zhao, Structure of cryptophyte photosystem II–light-harvesting antennae supercomplex, Nat. Commun. 15 (2024) 4999, http://dx.doi.org/10.1038/s41467-024-49453-0.

[76] W. Wang, L.-J. Yu, C. Xu, T. Tomizaki, S. Zhao, Y. Umena, X. Chen, X. Qin, Y. Xin, M. Suga, G. Han, T. Kuang, J.-R. Shen, Structural basis for blue-green light harvesting and energy dissipation in diatoms, Science 363 (6427) (2019) eaav0365, http://dx.doi.org/10.1126/science.aav0365, URL: https://www.science.org/doi/abs/10.1126/science.aav0365.

[77] L. Shen, Y. Gao, K. Tang, R. Qi, L. Fu, J.-H. Chen, W. Wang, X. Ma, P. Li, M. Chen, T. Kuang, X. Zhang, J.-R. Shen, P. Wang, G. Han, Structure of a unique PSII-Pcb tetrameric megacomplex in a chlorophyll d–containing cyanobacterium, Sci. Adv. 10 (2024) eadk7140, http://dx.doi.org/10.1126/sciadv.adk7140.

[78] A.O. Schouten, D.A. Mazziotti, Exciton-condensate-like energy transport in light-harvesting complex 2, PRX Energy 4 (2025) 013004, http://dx.doi.org/10.1103/PRXEnergy.4.013004.

[79] H. Sumi, Theory on rates of excitation-energy transfer between molecular aggregates through distributed transition dipoles with application to the antenna system in bacterial photosynthesis, J. Phys. Chem. B (ISSN: 1520-6106) 103 (1) (1999) 252–260, http://dx.doi.org/10.1021/jp983477u.

[80] H. Sumi, Structural strategies in the antenna system of photosynthesis on the basis of quantum-mechanical coherence among pigments, J. Lumin. (ISSN: 0022-2313) 87–89 (2000) 71–76, http://dx.doi.org/10.1016/S0022-2313(99)00232-X.

[81] H. Sumi, Bacterial photosynthesis begins with quantum-mechanical coherence, Chem. Rec. (ISSN: 1527-8999) 1 (6) (2001) 480–493, http://dx.doi.org/10.1002/tcr.10004.

[82] V.-R. Policht, A. Niedringhaus, R. Willow, P.-D. Laible, D.-F. Bocian, C. Kirmaier, D. Holten, T. Mancal, J.-P. Ogilvie, Hidden vibronic and excitonic structure and vibronic coherence transfer in the bacterial reaction center, Sci. Adv. 8 (1) (2022) http://dx.doi.org/10.1126/sciadv.abk0953, URL: https://www.science.org/doi/10.1126/sciadv.abk0953.

[83] B. González-Soria, F. Delgado, A. Anaya-Morales, Parametric mapping of quantum regime in fenna–matthews–olson light-harvesting complexes: A synthetic review of models, methods and approaches, Appl. Sci. 10 (18) (2020) 6474, http://dx.doi.org/10.3390/app10186474.

[84] N. Skochdopole, D.A. Mazziotti, Functional subsystems and quantum redundancy in photosynthetic light harvesting, J. Phys. Chem. Lett. 2 (23) (2011) 2989–2993, http://dx.doi.org/10.1021/jz201154t.

[85] H.-G. Duan, V.-I. Prokhorenko, R.-J. Cogdell, K. Ashraf, A.-L. Stevens, M. Thorwart, R.-J.-D. Miller, Nature does not rely on long-lived electronic quantum coherence for photosynthetic energy transfer, Proc. Natl. Acad. Sci. USA 114 (32) (2017) 8493–8498, http://dx.doi.org/10.1073/pnas.1702261114, URL: https://www.pnas.org/doi/epdf/10.1073/pnas.1702261114.

[86] M. Maiuri, E.-E. Ostroumov, R.-G. Saer, R.-E. Blankenship, G.-D. Scholes, Coherent wavepackets in the fenna-matthews-olson complex are robust to excitonic-structure perturbations caused by mutagenesis, Nat. Chem. 10 (2) (2018) 177–183, http://dx.doi.org/10.1038/NCHEM.2910, URL: https://www.nature.com/articles/nchem.2910.

[87] T. Scholak, F. de Melo, T. Wellens, F. Mintert, A. Buchleitner, Efficient and coherent excitation transfer across disordered molecular networks, Phys. Rev. E 83 (2, 1) (2011) http://dx.doi.org/10.1103/PhysRevE.83.021912, URL: https://journals.aps.org/pre/abstract/10.1103/PhysRevE.83.021912.

[88] T. Scholak, T. Wellens, A. Buchleitner, Optimal networks for excitonic energy transport, J. Phys. B: At. Mol. Opt. Phys. 44 (18, SI) (2011) http://dx.doi.org/10.1088/0953-4075/44/18/184012, URL: https://iopscience.iop.org/article/10.1088/0953-4075/44/18/184012.

[89] C.-C. Jumper, S. Rafiq, S. Wang, G.-D. Scholes, From coherent to vibronic light harvesting in photosynthesis, Curr. Opin. Chem. Biol. 47 (2018) 39–46, http://dx.doi.org/10.1016/j.cbpa.2018.07.023, URL: https://www.sciencedirect.com/science/article/pii/S1367593118300711.

[90] N.-N. Zhang, M.-J. Tao, W.-T. He, X.-Y. Chen, X.-Y. Kong, F.-G. Deng, N. Lambert, Q. Ai, Efficient quantum simulation of open quantum dynamics at various Hamiltonians and spectral densities, Front. Phys. 16 (5) (2021) http://dx.doi.org/10.1007/s11467-021-1064-y.

[91] X.-Y. Chen, N.-N. Zhang, W.-T. He, X.-Y. Kong, M.-J. Tao, F.-G. Deng, Q. Ai, G.-L. Long, Global correlation and local information flows in controllable non-Markovian open quantum dynamics, Npj Quantum Info. 8 (1) (2022) 22, http://dx.doi.org/10.1038/s41534-022-00537-z.

[92] S.-E. Braslavsky, E. Fron, H.-B. Rodriguez, E.-S. Roman, G.-D. Scholes, G. Schweitzer, B. Valeur, J. Wirz, Pitfalls and limitations in the practical use of forster's theory of resonance energy transfer, Photochem. Photobiol. Sci. 7 (12) (2008) 1444–1448, http://dx.doi.org/10.1039/b810620g.

[93] H. Dong, D.-Z. Xu, J.-F. Huang, C.-P. Sun, Coherent excitation transfer via the dark-state channel in a bionic system, Light. Sci. Appl. 1 (2012) http://dx.doi.org/10.1038/lsa.2012.2.

[94] C. Cohen-Tannoudji, Dark resonances from optical pumping to cold atoms and molecules, Phys. Scr. 90 (8) (2015) 088013, http://dx.doi.org/10.1088/0031-8949/90/8/088013, URL: https://iopscience.iop.org/article/10.1088/0031-8949/90/8/088013.

[95] J.-H. Kim, J. Cao, Optimal efficiency of self-assembling light-harvesting arrays, J. Phys. Chem. B 114 (49) (2010) 16189–16197, http://dx.doi.org/10.1021/jp106838k, URL: https://pubs.acs.org/doi/10.1021/jp106838k.

[96] R.-A. Miller, A.-D. Presley, M.-B. Francis, Self-assembling light-harvesting systems from synthetically modified tobacco mosaic virus coat proteins, J. Am. Chem. Soc. 129 (11) (2007) 3104–3109, http://dx.doi.org/10.1021/ja063887t.

[97] Y.-Z. Ma, R.-A. Miller, G.-R. Fleming, M.-B. Francis, Energy transfer dynamics in light-harvesting assemblies templated by the tobacco mosaic virus coat protein, J. Phys. Chem. B 112 (22) (2008) 6887–6892, http://dx.doi.org/10.1021/jp8006393, URL: https://pubs.acs.org/doi/10.1021/jp8006393.

[98] S. Mostarda, F. Levi, D. Prada-Gracia, F. Mintert, F. Rao, Structure-dynamics relationship in coherent transport through disordered systems, Nat. Commun. 4 (2013) 2296, http://dx.doi.org/10.1038/ncomms3296, URL: https://www.nature.com/articles/ncomms3296.

[99] D. Gfeller, P. De Los Rios, A. Caflisch, F. Rao, Complex network analysis of free-energy landscapes, Proc. Natl. Acad. Sci. USA 104 (6) (2007) 1817–1822, http://dx.doi.org/10.1073/pnas.0608099104, URL: https://www.pnas.org/doi/full/10.1073/pnas.0608099104.

[100] F.-D. Fuller, J. Pan, A. Gelzinis, V. Butkus, S.-S. Senlik, D.-E. Wilcox, C.-F. Yocum, L. Valkunas, D. Abramavicius, J.-P. Ogilvie, Vibronic coherence in oxygenic photosynthesis, Nat. Chem. 6 (8) (2014) 706–711, http://dx.doi.org/10.1038/NCHEM.2005, URL: https://www.nature.com/articles/nchem.2005.

[101] V. Butkus, D. Zigmantas, L. Valkunas, D. Abramavicius, Vibrational vs. electronic coherences in 2D spectrum of molecular systems, Chem. Phys. Lett. 545 (2012) 40–43, http://dx.doi.org/10.1016/j.cplett.2012.07.014, URL: https://www.sciencedirect.com/science/article/pii/S0009261412008044.

[102] V. Butkus, D. Zigmantas, D. Abramavicius, L. Valkunas, Distinctive character of electronic and vibrational coherences in disordered molecular aggregates, Chem. Phys. Lett. 587 (2013) 93–98, http://dx.doi.org/10.1016/j.cplett.2013.09.043, URL: https://www.sciencedirect.com/science/article/pii/S0009261413011986.

[103] E. Thyrhaug, K. Zidek, J. Dostal, D. Bina, D. Zigmantas, Exciton structure and energy transfer in the fenna-matthews-olson complex, J. Phys. Chem. Lett. 7 (9) (2016) 1653–1660, http://dx.doi.org/10.1021/acs.jpclett.6b00534, URL: https://pubs.acs.org/doi/10.1021/acs.jpclett.6b00534.

[104] P. Malý, V.-I. Novoderezhkin, R. van Grondelle, T. Mančal, Electron-vibrational coupling decreases trapping by low-energy states in photosynthesis, Chem. Phys. (ISSN: 0301-0104) 522 (2019) 69–76, http://dx.doi.org/10.1016/j.chemphys.2019.02.011, URL: https://www.sciencedirect.com/science/article/pii/S0301010418311133.

[105] M.-d. Rey, A.-W. Chin, S.-F. Huelga, M.-B. Plenio, Exploiting structured environments for efficient energy transfer: The phonon antenna mechanism, J. Phys. Chem. Lett. 4 (6) (2013) 903–907, http://dx.doi.org/10.1021/jz400058a.

[106] D.-A. Bryant, D.-P. Canniffe, How nature designs light-harvesting antenna systems: design principles and functional realization in chlorophototrophic prokaryotes, J. Phys. B: At. Mol. Opt. Phys. 51 (3) (2018) 033001, http://dx.doi.org/10.1088/1361-6455/aa9c3c.

[107] T. Meier, Y. Zhao, V. Chernyak, S. Mukamel, Polarons, localization, and excitonic coherence in superradiance of biological antenna complexes, J. Chem. Phys. 107 (10) (1997) 3876–3893, http://dx.doi.org/10.1063/1.474746, URL: http://dx.doi.org/10.1063/1.474746.

[108] M. Wendling, M. Przyjalgowski, D. Gülen, S. Vulto, T. Aartsma, R. van Grondelle, H. van Amerongen, The quantitative relationship between structure and polarized spectroscopy in the FMO complex of prosthecochloris aestuarii: refining experiments and simulations, Photosynth. Res. 71 (1–2) (2002) 99–123, http://dx.doi.org/10.1023/A:1014947732165, URL: https://link.springer.com/content/pdf/10.1023/A:1014947732165.

[109] K. Xiao, J. Liang, X. Wang, T. Hou, X. Ren, P. Yin, Z. Ma, et al., Panoramic insights into semi-artificial photosynthesis: Origin, development, and future perspective, Energy Env. Sci. 15 (2022) 529–549, http://dx.doi.org/10.1039/D1EE03094A.

[110] J. Liang, K. Xiao, X. Wang, T. Hou, C. Zeng, X. Gao, B. Wang, C. Zhong, Revisiting solar energy flow in nanomaterial–microorganism hybrid systems, Chem. Rev. 124 (2024) 9081–9112, http://dx.doi.org/10.1021/acs.chemrev.3c00831.

[111] J. Li, J. Shen, T. Hou, H. Tang, C. Zeng, K. Xiao, Y. Hou, B. Wang, A self-assembled MOF-Escherichia coli hybrid system for light-driven fuels and valuable chemicals synthesis, Adv. Sci. 11 (2024) 2308597, http://dx.doi.org/10.1002/advs.202308597.

[112] E.A. Hemmig, C. Creatore, B. Wünsch, L. Hecker, P. Mair, M.A. Parker, S. Emmott, P. Tinnefeld, U.F. Keyser, A.W. Chin, Programming light-harvesting efficiency using DNA origami, Nano Lett. 16 (4) (2016) 2369–2374, http://dx.doi.org/10.1021/acs.nanolett.5b05139.

[113] Y. Han, X. Zhang, Z. Ge, Z. Gao, R. Liao, F. Wang, A bioinspired sequential energy transfer system constructed via supramolecular copolymerization, Nat. Commun. 13 (2022) 3546, http://dx.doi.org/10.1038/s41467-022-31094-w.

[114] R. Haldar, M. Jakoby, A. Mazel, Q. Zhang, A. Welle, T. Mohamed, P. Krolla, W. Wenzel, S. Diring, F. Odobel, B.S. Richards, I.A. Howard, C. Wöll, Anisotropic energy transfer in crystalline chromophore assemblies, Nat. Commun. 9 (2018) 4332, http://dx.doi.org/10.1038/s41467-018-06829-3.

[115] B. Mu, X. Hao, X. Luo, Z. Yang, H. Lu, W. Tian, Bioinspired polymeric supramolecular columns as efficient yet controllable artificial light-harvesting platform, Nat. Commun. 15 (2024) 903, http://dx.doi.org/10.1038/s41467-024-45252-9.

[116] G. Amoruso, J. Liu, D.W. Polak, K. Tiwari, M.R. Jones, T.A.A. Oliver, High-efficiency excitation energy transfer in biohybrid quantum dot–bacterial reaction center nanoconjugates, J. Phys. Chem. Lett. 12 (23) (2021) 5448–5455, http://dx.doi.org/10.1021/acs.jpclett.1c01407.

[117] J. Liu, V.M. Friebe, R.N. Frese, M.R. Jones, Polychromatic solar energy conversion in pigment–protein chimeras that unite the two kingdoms of (bacterio)chlorophyll-based photosynthesis, Nat. Commun. 11 (2020) 1542, http://dx.doi.org/10.1038/s41467-020-15321-w.

[118] W. Song, Y. Liu, Y. Wu, C. Wang, Z. Liu, Y. Liu, X. Zhang, L. Cao, B. Li, B. Song, B. Cao, Y. Yao, X. Mao, Q. He, Z. Zou, B. Liu, Single-atom bridges across Biotic–abiotic interfaces facilitate direct electron transfer for solar-to-chemical conversion, Nat. Commun. 16 (2025) 6708, http://dx.doi.org/10.1038/s41467-025-62062-9.

[119] Z. Chen, H. Zhang, P. Guo, J. Zhang, G. Tira, Y.J. Kim, Y.A. Wu, Y. Liu, J. Wen, T. Rajh, J. Niklas, O.G. Poluektov, P.D. Laible, E.A. Rozhkova, Semi-artificial photosynthetic CO2 reduction through purple membrane re-engineering with semiconductor, J. Am. Chem. Soc. 141 (30) (2019) 11811–11815, http://dx.doi.org/10.1021/jacs.9b05564.